Nitric oxide mediates the pathogenesis of Marfan syndrome and a related aortic disease triggered by Adamts1 deficiency

Jorge Oller[1,9], Nerea Méndez-Barbero[1,9], E. Josue Ruiz[1], Silvia Villahoz[1], Marjolijn Renard[2], Lizet I. Canelas[1], Ana M. Briones[3], Rut Alberca[1], Noelia Lozano-Vidal[1], María A. Hurlé[4], Dianna Milewicz[5], Arturo Evangelista[6], Mercedes Salaices[3], J. Francisco Nistal[4], Luis Jesús Jiménez-Borreguero[7], Julie De Backer[3], Miguel R. Campanero[8,10], and Juan Miguel Redondo[1,10].

[1]Gene regulation in cardiovascular remodeling and inflammation group, Centro Nacional de Investigaciones Cardiovasculares (CNIC), Madrid, Spain; [2]Center for Medical Genetics Ghent, Ghent University Hospital, Ghent, Belgium; [3]Department of Pharmacology, Facultad de Medicina, Universidad Autónoma de Madrid, Madrid, Spain; [4]Cardiovascular Surgery and Department of Physiology and Pharmacology, Hospital Universitario Marqués de Valdecilla, IDIVAL, Facultad de Medicina, Universidad de Cantabria, Santander, Spain; [5]Division of Medical Genetics, University of Texas, Houston, USA; [6]Servei de Cardiologia, Hospital Vall d'Hebron, Barcelona, Spain; [7]CNIC and Hospital de la Princesa, Madrid, Spain; [8]Department of Cancer Biology, Instituto de Investigaciones Biomedicas Alberto Sols, CSIC-UAM, Madrid, Spain.

Corresponding authors contact information:
mcampanero@iib.uam.es and jmredondo@cnic.es

[9]Co-first authors
[10]Co-senior and corresponding authors

Abstract

Heritable thoracic aortic aneurysms and dissections (TAAD), including Marfan Syndrome (MFS), currently lack a cure, and causative mutations have been identified for only a fraction of affected families. Here, we identify ADAMTS1 and inducible nitric oxide synthase (NOS2) as therapeutic targets. We show that Adamts1 is a major mediator of vascular homeostasis whose genetic haploinsufficiency in mice causes a TAAD similar to MFS. Unexpectedly, aortic nitric oxide and Nos2 levels are increased in MFS mice and *Adamts1*-deficient mice before TGFß activation, and Nos2 inactivation protects these mice from developing aortopathy. More importantly, pharmacological inhibition of NOS2 rapidly and steadily reverses aortic dilation and medial degeneration in young *Adamts1*-deficient mice and in young and old MFS mice. MFS patients also show elevated NOS2 and downregulated ADAMTS1 in aorta, uncovering a possible causative role for this axis in human disease and urging evaluation of NOS2 inhibitors as a novel therapy.

Introduction

Aortic aneurysm (AA) and dissections account for 1–2% of all deaths in industrialized countries. Thoracic AA (TAA) is strongly associated with familial genetic predisposition and involves gene variants that show high penetrance. TAA and dissections (TAAD) can appear in isolation (Familial TAAD) or together with features of a systemic connective tissue disorder (syndromic TAAD), as in Marfan syndrome (MFS).

Syndromic and non-syndromic TAAD are associated with increased TGFß signaling[1-3]. TGFß activation is proposed to cause aortic medial degeneration, a typical histopathologic feature of TAAD characterized by an enlarged and weakened medial layer, fibrosis, proteoglycan accumulation, and elastic fiber disorganization and fragmentation[4]. However, it is unclear whether TGFß activation is cause or consequence of TAAD. Consistent with a pathogenic role of TGFß in TAAD, neutralizing anti-TGFß antibodies prevent aortic dilation and inhibit elastic lamellae fragmentation in a mouse model of mild MFS[5]. In the same model, these processes are also inhibited by losartan, an Angiotensin-II (Ang-II) type I receptor (AT1R) antagonist that inhibits TGFß signaling[5,6]. However, in clinical trials losartan was not more effective at reducing the rate of aortic root enlargement than the beta-blocker atenolol, and dual therapy with atenolol produced no additional benefit[7-9].

Little is known about the mechanisms by which Ang-II promotes aneurysm. We recently showed that Ang-II and other stimuli associated with vascular remodeling induce aortic expression of ADAMTS1 (A Disintegrin And Metalloproteinase with Thrombospondin Motifs 1)[10], thus raising the possibility that ADAMTS1 could mediate Ang-II-induced aneurysm. ADAMTS1, a member of the proteoglycan-degrading ADAMTS metalloproteinase family, is expressed in aortic endothelial and vascular smooth muscle cells (VSMCs)[11,12]. It is also expressed in TAA tissue and is active in normal aortic tissue, where it cleaves versican and aggrecan[13,14]. However, the role of Adamts1 in aneurysm development is unknown.

Results

Constitutive Adamts1 deficiency triggers a syndromic form of TAA.

To investigate the contribution of Adamts1 to Ang-II-elicited aortic dilation and aneurysm, we used *Adamts1*-deficient mice from the European Mouse Mutant Archive (EM: 02291). Previously described *Adamts1*$^{-/-}$ mice have congenital kidney malformations and high perinatal mortality[15], but no vascular phenotype has been reported. Our *Adamts1*$^{+/-}$ mice expressed lower levels of aortic Adamts1 than wild-type (wt) littermates (Fig.1a and Supplementary Fig. 1a). *Adamts1*$^{-/-}$ mice were not used because of their very low survival at weaning (Supplementary Fig 1b). In contrast, *Adamts1*$^{+/-}$ survival was similar to that of wt littermates, and these mice appeared healthy at this stage. Treatment of 8-week-old wt mice with Ang-II for 28 days promoted generalized aortic dilation, confirmed by ultrasonography of the aortic ring (AR), ascending aorta (AsAo) and abdominal aorta (AbAo) (Fig. 1b-1c). Unexpectedly, inactivation of 1 *Adamts1* allele induced aortic dilation in untreated mice, and this effect was exacerbated by Ang-II (Fig, 1b-1c). In addition, whereas Ang-II only induced AA or lethal aortic dissections in 1 of 11 wt mice, it quickly triggered their formation in 7 of 15 *Adamts1*$^{+/-}$ mice, 3 in the AsAo and 4 in the AbAbo (Fig. 1d-1e). No aneurysms or lethal dissections were detected in *Adamts1*$^{+/-}$ mice in the absence of Ang-II at this age. Since Ang-II induces hypertension, we investigated whether *Adamts1* inactivation had a similar effect. We found that, unlike Ang-II treatment, *Adamts1* gene dose reduction decreased systolic and diastolic blood pressure (BP) (Fig. 1f).

In line with developmental kidney abnormalities in other *Adamts1*-targeted mice[15], the kidneys of our *Adamts1*$^{+/-}$ mice had an enlarged caliceal space, indicating hydronephrosis (Supplementary Fig. 1c). However, plasma urea and creatinine were similar in wt and heterozygous mice (Supplementary Fig. 1d-1e), suggesting that renal function was not compromised.

The presence of renal abnormalities suggested that the aortic pathology induced by Adamts1 deficiency might be syndromic. Syndromic aortic conditions in humans and mice, including MFS, involve alterations to the lungs and skeleton[16-19]. Examination of 3-month-old

Adamts1$^{+/-}$ mice revealed a marked increase in distal airspace caliber, characteristic of emphysema (Fig. 1g). Significant kyphosis was detected in 44.4% of 3-4-month-old *Adamts1*$^{+/-}$ mice (Fig. 1h). This was associated with increased anteroposterior and transverse diameters of the chest due to overgrowth of the ribs (Fig. 1i). Other long bones (humerus, tibia and femur) were also longer in sex-matched *Adamts1*$^{+/-}$ mice, whereas cranial size and morphology showed no between-genotype differences (Fig. 1j-1k).

Aortic *Adamts1* knockdown promotes TAA.

To investigate the direct effects of Adamts1 depletion on aortic dilation, we knocked down its expression in the aorta of adult mice by using lentivirus encoding *Adamts1* specific siRNA. A screen of *Adamts1* siRNAs in cultured VSMCs identified the high silencing capacity of siRNA-27 (Supplementary Fig. 1f-1g). Lentiviral-driven coexpression of green fluorescent protein (GFP) facilitated assessment of transduction efficiency. Intrajugular delivery of lentivirus into C57BL/6 mice[20] yielded efficient and steady transduction of all aortic wall layers, determined by GFP immunostaining 7 weeks later of the AsAo, thoracic descending aorta, and AbAo (Fig. 2a-2b and Supplementary Fig. 1i). The expression of Adamts1 was almost undetectable in aortic samples of mice inoculated with lentivirus encoding *siRNA-27* (*siAdamts1*) (Fig. 2b-2c and Supplementary Fig. 1h-1i), even when mice were treated with Ang-II for the last 4 weeks (Fig. 2c and Supplementary Fig 1i). Indeed, *Adamts1* mRNA levels in aortic samples of transduced mice were below those in *Adamts1*$^{+/-}$ aorta (Supplementary Fig. 1i). Adamts1 silencing was confirmed in all layers of the AsAo, thoracic descending aorta, and AbAo (Fig. 2b and Supplementary Fig. 1h). Consistent with the data from *Adamts1*$^{+/-}$ mice, *Adamts1* silencing in adult aorta decreased systolic and diastolic BP (Fig. 2d) and induced strong dilation of the AR, AsAo, and AbAo that was further increased by treatment with Ang-II (Fig. 2e and Supplementary Fig 1j). In addition, Ang-II treatment of mice transduced with *siAdamts1* caused aneurysm in 13 of 16 as well as lethal dissections (4 of 16), whereas only 1 of 13 mice transduced with a control siRNA (*siCtl*) and treated with Ang-II formed aneurysms and none developed lethal dissections. No aneurysms or lethal dissections were detected in *siAdamts1* mice in the absence of Ang-II at this age.

Medial degeneration and activation of the TGFß pathway in the aortic wall of *Adamts1* deficient mice.

Histologic analysis of the AsAo and the AbAo revealed that reduction of Adamts1 levels, by lentiviral transduction or genetic inactivation, caused the characteristic features of medial degeneration: elastic-fiber fragmentation and disarray, excessive collagen deposition, and proteoglycan accumulation (Fig 2f-2h and Supplementary Fig. 2a-2e). These features were exacerbated by Ang-II (Fig 2f-2h and Supplementary Fig. 2a-2e).

Aortic medial degeneration in Marfan and Loeys-Dietz syndromes is linked to activation of the TGFß pathway[17,21]. The activation of this pathway leads to phosphorylation of the transcription factors Smad2/3, their subsequent translocation to the nucleus and the transcriptional induction of their target genes, including *Ctgf*, *Col1a1*, and *Pai-1.* Immunohistochemistry of aortic sections from *Adamts1*$^{+/-}$ mice revealed increased TGFß1 and Smad2/3 expression (Fig 2i) and increased Smad2 activation, determined by elevated phosphorylation and nuclear location (Fig 2i). Similar results were found in *Adamts1* knock-down mice (Supplementary Fig. 3a). Increased Smad2/3 expression and Smad2 activation were also confirmed by immunofluorescence of sections from the AsAo of *Adamts1*$^{+/-}$ mice and was similar to that found in aortic sections from a mouse model of Marfan syndrome Supplementary Fig. 3b), a mouse heterozygous for an *Fbn1* allele including a cysteine substitution (*C1039G*)[18], equivalent to a mutation frequent in MFS patients. Consistently, aortas of *Adamts1*$^{+/-}$ and *siAdamts1*-inoculated mice had elevated mRNA levels of the TGFß transcriptional targets *Ctgf*, *Col1a1*, and *Pai-1* (Supplementary Fig. 3c-3d).

Aortic dilation induced by *Adamts1* deficiency is fast and independent of TGFß

To assess the pathogenesis of Adamts1-deficiency-dependent baseline aortopathy, we monitored AsAo and AbAo diameter and BP after intrajugular inoculation of *siCtl* or *siAdamts1* lentiviruses (Fig. 3a). Reduced *Adamts1* mRNA and protein levels were detected from as early as 1-2 days post-inoculation (Fig. 3b and Supplementary Fig. 4a), and were immediately followed by BP drop and elastolysis induction (Fig. 3c-3d and Supplementary Fig. 4b-4c). The aortic diameter did not increase significantly until 3 days post-inoculation

(Fig. 3e). These events preceded collagen deposition in the aortic wall (Fig. 3f) and transcriptional activation of the TGFß pathway, which began 1-2 weeks post-inoculation (Supplementary Fig. 4d). The early induction of elastolysis prompted us to assess the activity of Mmp2 and Mmp9, major elastolytic proteins in the aortic wall. Activity of Mmp9, but not Mmp2, was rapidly and markedly induced after *Adamts1* silencing (Fig. 3g). Consistently, Immunofluorescence staining of Mmp9 in AsAo sections revealed increased levels in the tunica media, coinciding with smooth muscle actin-positive cells (Fig. 3h). Notably, macrophages, a known source of Mmp9 in inflammatory diseases, were almost absent from these aortic sections (Fig. 3h) but were readily detected in atheroma plaques from *Apoe*$^{-/-}$ mice[22] (Fig. 3h).

Canonical and non-canonical pathways of TGFß activation play critical roles in a mouse model of MFS, and a TGFß-neutralizing antibody and the AT1R antagonist losartan can both prevent aneurysm formation in this model[5]. Although the timing of TGFß activation after Adamts1 silencing suggested a secondary role in aortopathy onset, we used losartan and a TGFß-neutralizing antibody to assess the contribution of the TGFß pathway (Fig. 3i). Strikingly, neither treatment inhibited aortic dilation induced by *siAdamts1* (Fig. 3j and Supplementary Fig. 4e). Moreover, these treatments did not prevent hypotension (Supplementary Fig. 4f) and did not reduce elastic fiber fragmentation or fibrosis (Fig 3k-3l). To confirm that the neutralizing antibody was correctly administered and worked efficiently, we determined mRNA levels of TGFß transcriptional targets and found that the TGFß antibody efficiently inhibited induction of *Tgfb1*, *Pai-I, Ctgf*, and *Col1a1* (Supplementary Fig. 4g). These results also indicate that fibrosis is independent of TGFß activation during disease onset. Losartan, as expected, reduced BP in control mice (Supplementary Fig. 4f). These results support the conclusion that TGFß pathway activation is secondary to aortic dilation and elastolysis in Adamts1-related aortopathy.

Nos2-derived nitric oxide mediates the aortopathy induced by *Adamts1* deficiency

To further investigate the mechanism of Adamts1-related aortopathy, we focused on potential mediators of hypotension, the earliest effect detected upon *Adamts1* silencing. A

candidate factor is nitric oxide (NO), an endogenous vasorelaxant that relaxes smooth muscle and lowers BP. NO can be produced by constitutively expressed NO synthase (NOS) of endothelial (eNOS, NOS3) or neuronal (nNOS, NOS1) origin or by inducible NOS (iNOS, NOS2)[23]. To test the contribution of NO to the induction of aortic dilation, we treated C57BL/6 mice with NΩ-nitro-L-arginine-methylesther (L-NAME), an inhibitor of all NOS enzymes (Fig. 4a). Despite its hypertensive effect (Supplementary Fig. 5a), L-NAME prevented *siAdamts1*-induced dilation of the AsAo and the AbAo (Fig. 4b), blocked elastolysis (Fig, 4c and Supplementary Fig. 5b), decreased the fibrosis (Fig. 4d) and prevented Mmp9 activation (Fig. 4e).

To determine the therapeutic potential of NOS activity inhibition, we administered L-NAME to *Adamts1*$^{+/-}$ mice. L-NAME rapidly decreased AsAo and AbAo diameter to normal levels (Fig. 4f), increased BP (Fig 4g and Supplementary Fig. 5c), decreased elastic fiber fragmentation (Fig 4h), and diminished fibrosis (Fig 4i).

Under physiological conditions, vascular NOS3 produces low levels of NO to maintain vascular homeostasis[24], whereas under pathological conditions NOS2 can be transcriptionally activated and produce 1000-fold more NO than its constitutive counterparts[25]. We therefore hypothesized that Nos2 levels might be increased in Adamts1 deficient mice and mediate aortic dilation and medial degeneration. *Nos2* expression was significantly induced as early as 2 days after *siAdamts1* inoculation, whereas Nos3 was unaffected (Supplementary Fig. 5d). *Endothelin-1*, another BP regulator, was not affected by *Adamts1* silencing (Supplementary Fig. 5d). Immunostaining of aortic cross sections from *siAdamts1* and *Adamts1*$^{+/-}$ mice confirmed increased Nos2 levels in the medial layer coinciding with smooth muscle actin-positive cells (Fig. 5a).

To investigate whether Nos2-derived NO mediates the aortopathy induced by Adamts1 deficiency, we inoculated *Nos2*$^{+/+}$ and *Nos2*$^{-/-}$ mice with *siAdamts1* lentivirus (Fig. 5b). *Nos2*-deficiency blocked si*Adamts1*-induced AsAo and AbAo dilation (Fig. 5c and Supplementary Fig. 5e), elastic fiber fragmentation (Fig. 5d and Supplementary Fig. 5f) and fibrosis (Fig. 5e). *Nos2*$^{-/-}$ mice were normotensive and *Adamts1* silencing failed to decrease

their systolic and diastolic BP (Fig. 5f and Supplementary Fig. 5g). Consistent with a critical role for Nos2-derived NO in Adamts1-deficiency-induced aortopathy, unfixed sections of *siAdamts1*-transduced aorta contained higher NO levels than sections from control mice (Fig. 5g). Similarly, NO levels were higher in unfixed sections of *Adamts1*$^{+/-}$ aorta than in those from wt mice (Fig. 5g). NO did not accumulate in aortic sections of *Nos2*$^{-/-}$ mice inoculated with *siAdamts1* (Fig. 5g).

Since Akt is a mediator of Nos2 induction[26] and is activated by Syndecan-4, a known proteolytic Adamts1 target[27], we investigated the contribution of Akt to the induction of Nos2 by Adamts1 insufficiency. Phosphorylation of Akt, a marker of its activation, was increased in aortic protein extracts from mice inoculated with *siAdamts1* lentiviruses (Figure 5h). NF-kB, a critical transcription factor for *Nos2* induction[28], was also activated following *Adamts1* silencing, as determined by phosphorylation of its p65 subunit (Fig. 5h). In addition, *in vitro* transduction of VSMCs with *siAdamts1* lentiviruses induced Akt and NF-kB activation and Akt-dependent Nos2 expression (Supplementary Fig. 5h-5j). Moreover, pharmacological inhibition of Akt activation in *Adamts1*$^{+/-}$ mice with the mTOR inhibitor AZD8055 rapidly and markedly decreased aortic dilation to normal levels, inhibited NO production in the aortic wall, and reduced *Nos2* levels (Fig 5i-5l). Finally, in agreement with the Nos2 upregulation in cultured VSMCs, *in vitro* transduction of these cells with *siAdamts1* lentiviruses sharply increased the levels of NO-derived metabolites (Supplementary Fig. 5k) and readily induced NO production (Supplementary Fig. 5l). Together, these results strongly suggest that Akt activation mediates Nos2 induction in the dilated aortic wall.

Nitric oxide and Adamts1 play a critical role in Marfan syndrome

We hypothesized that NO might mediate medial degeneration in other syndromic forms of TAAD. To determine the role of NO in MFS, we administered L-NAME to the *Fbn1*$^{C1039G/+}$ MFS mouse model (Supplementary Fig 6a). The *Fbn1*$^{C1039G/+}$ phenotype resembles human MFS, including aortic dilation, aneurysm and dissection, and histological features of aortic medial degeneration[18]. Twelve-week-old *Fbn1*$^{C1039G/+}$ mice exhibited dilation of the AsAo and AbAo (Supplementary Fig. 6b) similar to that of Adamts1-deficient mice. L-

NAME rapidly decreased the AsAo and AbAo diameters to normal levels (Supplementary Fig. 6b), augmented systolic and diastolic BP (Supplementary Fig. 6c), and diminished elastic fiber fragmentation (Supplementary Fig. 6d). *Fbn1*$^{C1039G/+}$ mice showed no significant collagen accumulation, and collagen content was unaffected by L-NAME (Supplementary Fig. 6e).

Fbn1$^{C1039G/+}$ mice also exhibited markedly elevated levels of Nos2 and NO production relative to littermate controls (Fig 6a and Supplementary Fig. 7a), while *Nos3* was unaffected (Supplementary Fig. 7a). To determine whether Nos2 induction in these mice has a pathogenic role, we generated *Fbn1*$^{C1039G/+}$*;Nos2*$^{-/-}$ mice, finding that their AsAo and AbAo diameters were markedly smaller than those of *Fbn1*$^{C1039G/+}$ mice (Supplementary Fig 7b).

The similarities between *Adamts1*$^{+/-}$ and *Fbn1*$^{C1039G/+}$ mice suggested a link between Adamts1 and the aortic pathology of *Fbn1*$^{C1039G/+}$ mice. Immunostaining of *Fbn1*$^{C1039G/+}$ aortic sections revealed reduced levels of Adamts1 (Fig. 6b), confirmed by immunoblot analysis of aortic protein extracts (Fig. 6b). However, *Adamts1* mRNA levels were similar in *Fbn1*$^{C1039G/+}$ mice and control littermates (Fig. 6c), suggesting posttranscriptional downregulation of Adamts1 expression in Marfan syndrome.

Assessment of the contribution of ADAMTS1 and NOS2 to human MFS revealed depressed ADAMTS1 expression in the medial layer of aortic sections from MFS patients compared with aortas from organ transplant donors, regardless of sex and age (Fig. 6d and Supplementary Fig. 7c). Quantification of the ADAMTS1-positive area in immunohistochemistry-stained sections confirmed a marked expression decrease in MFS samples (Fig. 6e). Elastin autofluorescence was barely detected in MFS aortic sections and showed a disorganized pattern (Fig. 6d). NOS2 immunofluorescence revealed higher expression in the medial layer of 6 out of 8 MFS aortic sections (Fig. 6d and Supplementary Fig. 7d) and quantification of NOS2-positive area in these sections showed a sharp increase in MFS samples (Fig. 6f). Of note, SMA immunofluorescence of these sections indicated that NOS2 was induced in VSMCs from MFS patients (Supplementary Fig. 7e).

Since L-NAME increases BP, likely through its inhibition of Nos3, it is unsuitable for the long-term treatment of TAA. To investigate whether drugs targeting only the inducible NOS isoform might be of therapeutic interest for syndromic TAA, we treated cultured *siAdamts1*-transduced VSMCs with 1400W, a potent and highly specific inhibitor of NOS2[29], and found that it blocked NO and nitrites production (Supplementary Fig. 5k-5l). We then treated 12-week-old *Adamts1*$^{+/-}$ and *Fbn1*$^{C1039G/+}$ mice for 16 weeks with 1400W. This longitudinal study revealed a rapid decrease in AsAo and AbAo diameters to normal levels that was maintained throughout the treatment period (Fig 6g and Supplementary Fig 8a). The efficiency of 1400W in reducing aortic dilation was confirmed by *ex vivo* measurement (Supplementary Fig 8b). Notably, this treatment did not increase BP in these mice above normal levels (Fig 6h and Supplementary Fig. 8c) and did not appear to have significant effects on the health of these mice. Histological analysis of aortic cross-sections showed almost complete regression of elastic fiber fragmentation (Fig 6i and Supplementary Fig 8d-8e). To determine whether NOS2 inhibition was also effective in older mice, we treated 9-month-old *Fbn1*$^{C1039G/+}$ mice with 1400W, finding that aortic diameter decreased rapidly to normal levels (Fig 6j and Supplementary Fig 8f) with no increase in BP above normal levels (Figure 6k). Together, these data support the notion that ADAMTS1 and NOS2 might be important mediators of the aortic pathology in human MFS (Fig. 6l) and warrant evaluation of NOS2 inhibitors for the treatment of syndromic TAA.

Discussion

This study identifies NO as an essential mediator of syndromic aortic diseases in mouse models and suggests it as a possible target for intervention in human aortopathies. In addition, we show that Adamts1 is an important mediator of vascular wall homeostasis whose expression is decreased in MFS. The resemblance of the aortopathy in *Adamts1*-deficient mice to human syndromic FTAAD suggests that the ADAMTS1 downregulation in MFS may underlie the aortic phenotype of MFS patients. The extent of the aortic dilatation is similar in young *Adamts1*-insufficient and Marfan mice, and the elastic fibers are severely compromised in both mouse models. None of these mice developed aneurysm at this age, but administration of the hypertensive factor Ang-II for less than 1 month induced aneurysms in nearly 80% of *Adamts1*-insufficient mice and lethal aortic dissections in almost 50%. The aortic dilation and medial degeneration induced by *Adamts1* deficiency might resemble the early stages of human disease, while the exacerbation of the aortic pathology induced by Ang-II in mice likely mimics later stages of human aortic diseases, when their course is worsened by aging-related hypertension.

Since ADAMTS1 levels are upregulated by AngII[10], we hypothesized that ADAMTS1 was an important mediator of AngII-induced aortic disease. However, partial Adamts1 deficiency, far from protecting the aortic wall, caused its pathological remodeling, indicating a homeostatic role for Adamts1. Studies in other Adamts1-deficient mice did not report this vascular role[15,30,31]. It will be therefore interesting to investigate the aortic heterozygous and homozygous phenotype in these models, and determine whether the different genetic backgrounds used (pure C57BL/6 mice here versus the mixed background used in earlier studies) account for the observed differences in lethality and fertility.

Mutations in several ADAMTS and ADAMTS–like (ADAMTSL) family members implicated in microfibril formation have been linked to connective tissue disorders without an aortic phenotype[32]. These disorders are similar to others produced by mutation of residues in *FBN1*, the major tissue microfibril component[33], suggesting that interaction of ADAMTS proteins with fibrilins may be crucial to the regulation of connective tissue homeostasis. In

light of our results, an attractive idea is that FBN1 mutations linked to MFS might disrupt domains required for interaction with ADAMTS1; in such a scenario, loss of this interaction could destabilize ADAMTS1, thus explaining its low levels in MFS patients and the shared features of *Adamts1*$^{+/-}$ and MFS mice.

We previously reported that lentivirus tropism depends on the administration route[34] and that injection into the jugular vein yields stable and efficient transduction of the aortic wall[20]. This approach achieves long-term silencing of Adamts1 throughout the aorta and results in aortic phenotypic changes and symptoms indistinguishable from those of *Adamts1*$^{+/-}$ mice. Timed knockdown enabled us to define the pathological sequence leading to disease: *siAdamts1* transduction triggered immediate hypotension and elastolysis, followed rapidly by aortic dilation, whereas the TGFß-Smad pathway was not activated until 1-2 weeks after lentiviral infection.

Although aortic medial degeneration and dilation are associated with activation of the TGFß and AngII pathways in syndromic and non-syndromic aortic disease[4,17,21,35], blockade of these pathways had no significant effect on *siAdamts1*-mediated aortic dilation, medial degeneration or hypotension, at least in the first 2 weeks of disease. Our data are nonetheless compatible with a role for these pathways at later stages. In this regard, TGFß neutralization also failed to inhibit aneurysm progression at the early stages of a progressively severe form of MFS (*Fbn1*$^{mgR/mgR}$ mice), but was protective at later stages[36].

Hypertension is considered a risk factor in AA; however, our results show that the hypertensive effects of L-NAME are compatible with reversal of aortic dilation in *Adamts1*$^{+/-}$ and MFS mice. Reversal of dilation was remarkably fast, being complete in 1 week. Elastic fiber and collagen deposition in *Adamts1*$^{+/-}$ mice returned to normal levels 3 weeks after NOS inhibition, suggesting activation of mechanisms for collagen clearance from the aortic wall and the induction of elastin synthesis. Since NO is a critical regulator of smooth muscle cell contractility, we propose that the rapid dilation after *Adamts1* knockdown and the rapid regression of the aortic diameter after treatment with NO inhibitors suggest that dilation is strongly dependent on cell contractility and that the structural changes are a consequence of

the dysregulation of the contractile mechanism. Our results suggest that NO is a primary trigger of syndromic aortic disease and is also required to sustain its symptoms. Short-term treatment with NO donors, as established for angina, is unlikely to cause aortic damage; however, our findings indicate the need for caution in implementing long-term treatments with NO donors or gene-therapy-augmented NOS expression.

A recent report showed that gain-of-function mutations in *PRKG1*, a downstream target of NO, are present in 4 families affected by TAA[37], suggesting that NO might be also essential in non-syndromic, familial TAAD. The increased PKG1 activity promoted activation of the myosin regulatory light chain phosphatase and thus was predicted to decrease the VSMC contractility[37]. A critical role of the NO signaling pathway in maintaining VSMC contractility is consistent with the association of familial TAAD with mutations in other genes involved in the regulation of the VSMC contractile unit, including ACTA2, MYH11, and MYLK[38]. It will be important to determine whether the NO pathway also operates in the aortic disease associated with these mutations.

A number of substrates, such as aggrecan, versican, syndecan4, semaphorin 3C, nidogen-1 and -2, and desmocollin-3, are proteolytically degraded by ADAMTS1[39] and are therefore candidate mediators of its vascular homeostatic functions. The accumulation of any of these substrates in ADAMTS1-deficient tissues might also mediate the pathogenesis induced by Adamts1 insufficiency. Indeed, high levels of syndecan4 lead to activation of Akt[27], a kinase known to activate NF-kB[40]. Akt and NF-kB are known mediators of *NOS2* induction[27,28] and we have shown that both are activated early after *Adamts1* knockdown in aortic tissue and in cultured VSMCs, concomitantly with Nos2 induction. We therefore propose that Akt and NF-kB could mediate Nos2 induction elicited by Adamts1 insufficiency. Accordingly, pharmacological inhibition of mTOR/Akt markedly and rapidly decreased *Nos2* levels and NO production in the aortic wall and regressed aortic dilation in *Adamts1*$^{+/-}$ mice to normal levels. Although mTOR/Akt inhibitors would also appear to be alternative therapeutic tools for aortic dilation, they are upstream components of many signaling pathways, including

those regulating cell survival. A further analysis of the long-term effect of these drugs will be required before considering them as therapeutic alternatives in aortic diseases

NOS2-mediated increases in NO might activate Mmp9-dependent elastin fragmentation, thus initiating medial degeneration. Supporting this idea, Mmp9 activation and elastin fragmentation are sensitive to NOS inhibition in the aorta of *Adamts1*-deficient mice. Although we cannot exclude involvement of other proteinases in the elastolytic processes of pathological aortic dilation, Mmp9 is an important elastolytic metalloproteinase and a target of NO regulation[41,42]. *Adamts1* silencing identified early activation of Mmp9, but not Mmp2, in the onset of aortic disease, a pattern typical of macrophages. However, we show that Mmp9 is expressed in the medial layer by VSMCs and that macrophages are almost absent from this layer. We therefore propose that VSMCs are a major source of Mmp9 in this context. These results are consistent with previous findings showing that inflammatory cells are scarce in aortas of MFS patients[43]. Indeed, inflammation has been documented in only a small number of cases of human TAA[44-46]. Notably, two reports showing high ADAMTS1 levels in the aorta of TAA patients also showed the presence of inflammatory cells in the vessel wall[13,47] and high levels of ADAMTS1 in macrophages and neutrophils[47]. It thus seems likely that syndromic TAAD and inflammatory TAAD express opposed ADAMTS1 levels and are mechanistically distinct.

Previous reports implicating NO in mouse models of cerebral and abdominal AA provide contradictory data, often related to pharmacological versus targeted genetic deletion approaches. For example, inhibitory or stimulatory roles for Nos2 have been reported in models of AAA[48-52]. In cerebral aneurysm, results with pharmacological inhibitors indicate that Nos2 is critical for disease development[53]; however, the incidence of cerebral aneurysm is similar in *Nos2*$^{-/-}$ and wt mice[54]. In our analysis, the genetic studies support the results obtained with L-NAME and the NOS2-specific inhibitor 1400W: *Nos2*$^{-/-}$ mice were resistant to *siAdamts1*-triggered aortopathy, and *Fbn1*$^{C1039G/+}$;*Nos2*$^{-/-}$ mice showed no aortic dilation. The pathological role of NO in these models is thus mediated by Nos2, which is induced as early as 2 days after *Adamts1* silencing.

Although Nos2 is not normally expressed in resting cells, once induced it remains highly active[23]. We show high Nos2 protein in 2 mouse models of *Adamts1* deficiency, in MFS mice, and, more importantly, in aortic sections of MFS patients. Together our results suggest that NOS2-mediated NO production plays an essential role in the pathogenesis of MFS and the aorthopathy triggered by *Adamts1* deficiency (Fig. 6l). The *Adamts1* deficiency in MFS mice and human patients indicates that these aortic diseases are likely linked mechanistically, and suggests that *Adamts1* deficiency may partially or fully explain the aortic phenotype of MFS.

The current standard treatment for MFS, ß-adrenergic blockers, slow aortic dilation but do not prevent dissection[55]. The AT1R antagonist losartan ameliorated aortic growth and controlled TGFß pathway activation in mouse models of MFS, thus raising high expectations for MFS therapy. However, several recent clinical trials show that the ß-adrenergic blocker atenolol is as or more effective than losartan at reducing aortic growth in MFS[7-9,56]. Although caution should be exercised in extrapolating conclusions obtained in mouse models to human disease, the powerful and extremely fast action of NOS2 inhibition in reversing aortopathies in mouse models warrants preclinical and clinical trials with drugs that target the NO pathway for the treatment of MFS and other aortic diseases. The NOS2 inhibitor 1400W was equally effective in young and relatively old mice, suggesting that Nos2 is a critical pathogenic mediator not only in the context of disease initiation, but also in later disease progression. Long-term use of 1400W provided a sustained protection of the aorta in our mouse models and showed no evidence of side effects. Considering that NOS2 inhibitors have been safely used in clinical trials of endotoxemia, rheumathoid arthritis and migraine (ClinicalTrials.gov Identifiers: NCT00184990, NCT00370435, NCT00242866), our results point to specific NOS2 inhibitors as a promising alternative for the treatment of aortic disease that could be implemented with minimal delay.

ACKNOWLEDGMENTS

We thank B Ibañez and G Egea for reagents; S Bartlett for English editing; AG Arroyo, S Lamas, J Alegre-Cebollada and J Ruiz-Cabello for critical reading of the manuscript and advice; and S Pocock and J Vazquez for advice on statistics. We also thank the CNIC histology facility, C Velasco, AV Alonso and L Flores for technical support. The Spanish Ministerio de Economía y Competitividad (MINECO) supports MRC with grant SAF2013-45258P and and JMR with grants SAF2012-34296 and SAF2015-636333R. JMR and AE are also funded by Fundacion La Marato TV3 grants 20151330, /31. MRC is also supported by CSIC. The Red de Investigación Cardiovascular (RIC) of Ministerio de Sanidad supports the research of JMR, AE, MS, JLJ-B and JFN with grants RD12/0042/0022, /0021, /0024, /0056 and /0018. CNIC is supported by MINECO and Pro-CNIC Foundation, and is a Severo Ochoa Center of Excellence (MINECO award SEV-2015-0505). EJR, JO, and SV hold, respectively, a Marie Skłodowska-Curie fellowship and FPI fellowships BES 2010-034552 and SVP-2013-067777. The cost of this publication has been paid in part with FEDER funds. The authors have no conflict of interest to declare.

AUTHOR CONTRIBUTIONS

The study was conceived by MRC and JMR. JO, NMB, MRC and JMR designed the study and analyzed the data. JO and NMB performed most of the experiments, with contributions from EJR, SV, LI, RA and NL-V. LJJ-B supervised and analyzed echography analysis. MR, JDB, MAH, and JFN provided human tissue samples. LJJB, MR, AB, MAH, DM, AE, MS, JFN, and JDB provided experimental support and ideas for the project. MRC and JMR wrote the manuscript with contributions of JO and NMB. All authors read and approved the manuscript.

EXTENDED DATA

Extended Data includes eight additional figures.

REFERENCES

1 Dietz, H. C. TGF-beta in the pathogenesis and prevention of disease: a matter of aneurysmic proportions. *J Clin Invest* **120**, 403-407, (2010).

2 Gallo, E. M. *et al.* Angiotensin II-dependent TGF-beta signaling contributes to Loeys-Dietz syndrome vascular pathogenesis. *J Clin Invest* **124**, 448-460, (2014).

3 Renard, M. *et al.* Novel MYH11 and ACTA2 mutations reveal a role for enhanced TGFbeta signaling in FTAAD. *Int J Cardiol* **165**, 314-321, (2013).

4 Gillis, E., Van Laer, L. & Loeys, B. L. Genetics of thoracic aortic aneurysm: at the crossroad of transforming growth factor-beta signaling and vascular smooth muscle cell contractility. *Circ Res* **113**, 327-340, (2013).

5 Habashi, J. P. *et al.* Losartan, an AT1 antagonist, prevents aortic aneurysm in a mouse model of Marfan syndrome. *Science* **312**, 117-121, (2006).

6 Lim, D. S. *et al.* Angiotensin II blockade reverses myocardial fibrosis in a transgenic mouse model of human hypertrophic cardiomyopathy. *Circulation* **103**, 789-791 (2001).

7 Forteza, A. *et al.* Efficacy of losartan vs. atenolol for the prevention of aortic dilation in Marfan syndrome: a randomized clinical trial. *Eur Heart J*, (2015).

8 Lacro, R. V. *et al.* Atenolol versus losartan in children and young adults with Marfan's syndrome. *N Engl J Med* **371**, 2061-2071, (2014).

9 Milleron, O. *et al.* Marfan Sartan: a randomized, double-blind, placebo-controlled trial. *Eur Heart J* **36**, 2160-2166, (2015).

10 Oller, J. *et al.* C/EBPbeta and Nuclear Factor of Activated T Cells Differentially Regulate Adamts-1 Induction by Stimuli Associated with Vascular Remodeling. *Mol Cell Biol* **35**, 3409-3422, (2015).

11 Luque, A., Carpizo, D. R. & Iruela-Arispe, M. L. ADAMTS1/METH1 inhibits endothelial cell proliferation by direct binding and sequestration of VEGF165. *J Biol Chem* **278**, 23656-23665, (2003).

12 Thai, S. N. & Iruela-Arispe, M. L. Expression of ADAMTS1 during murine development. *Mech Dev* **115**, 181-185 (2002).

13 Ren, P. *et al.* ADAMTS-1 and ADAMTS-4 levels are elevated in thoracic aortic aneurysms and dissections. *Ann Thorac Surg* **95**, 570-577, (2013).

14 Sandy, J. D. *et al.* Versican V1 proteolysis in human aorta in vivo occurs at the Glu441-Ala442 bond, a site that is cleaved by recombinant ADAMTS-1 and ADAMTS-4. *J Biol Chem* **276**, 13372-13378, (2001).

15 Mittaz, L. *et al.* Adamts-1 is essential for the development and function of the urogenital system. *Biol Reprod* **70**, 1096-1105, (2004).

16 Cohn, R. D. *et al.* Angiotensin II type 1 receptor blockade attenuates TGF-beta-induced failure of muscle regeneration in multiple myopathic states. *Nat Med* **13**, 204-210, (2007).

17 Neptune, E. R. *et al.* Dysregulation of TGF-beta activation contributes to pathogenesis in Marfan syndrome. *Nat Genet* **33**, 407-411, (2003).

18 Pereira, L. *et al.* Pathogenetic sequence for aneurysm revealed in mice underexpressing fibrillin-1. *Proc Natl Acad Sci U S A* **96**, 3819-3823 (1999).

19 Pyeritz, R. E. The Marfan syndrome. *Annu Rev Med* **51**, 481-510, (2000).

20 Esteban, V. *et al.* Regulator of calcineurin 1 mediates pathological vascular wall remodeling. *J Exp Med* **208**, 2125-2139, (2011).

21 Loeys, B. L. *et al.* A syndrome of altered cardiovascular, craniofacial, neurocognitive and skeletal development caused by mutations in TGFBR1 or TGFBR2. *Nat Genet* **37**, 275-281, (2005).

22 Mendez-Barbero, N. *et al.* A major role for RCAN1 in atherosclerosis progression. *EMBO Mol Med* **5**, 1901-1917, (2013).

23 Forstermann, U. & Sessa, W. C. Nitric oxide synthases: regulation and function. *Eur Heart J* **33**, 829-837, 837a-837d, (2012).

24 Albrecht, E. W., Stegeman, C. A., Heeringa, P., Henning, R. H. & van Goor, H. Protective role of endothelial nitric oxide synthase. *J Pathol* **199**, 8-17, (2003).

25 Pfeilschifter, J., Eberhardt, W. & Beck, K. F. Regulation of gene expression by nitric oxide. *Pflugers Arch* **442**, 479-486 (2001).
26 Tang, C. H., Lu, D. Y., Tan, T. W., Fu, W. M. & Yang, R. S. Ultrasound induces hypoxia-inducible factor-1 activation and inducible nitric-oxide synthase expression through the integrin/integrin-linked kinase/Akt/mammalian target of rapamycin pathway in osteoblasts. *J Biol Chem* **282**, 25406-25415, (2007).
27 Partovian, C., Ju, R., Zhuang, Z. W., Martin, K. A. & Simons, M. Syndecan-4 regulates subcellular localization of mTOR Complex2 and Akt activation in a PKCalpha-dependent manner in endothelial cells. *Mol Cell* **32**, 140-149, (2008).
28 Kleinert, H., Schwarz, P. M. & Forstermann, U. Regulation of the expression of inducible nitric oxide synthase. *Biol Chem* **384**, 1343-1364, (2003).
29 Garvey, E. P. *et al.* 1400W is a slow, tight binding, and highly selective inhibitor of inducible nitric-oxide synthase in vitro and in vivo. *J Biol Chem* **272**, 4959-4963 (1997).
30 Lee, N. V. *et al.* Fibulin-1 acts as a cofactor for the matrix metalloprotease ADAMTS-1. *J Biol Chem* **280**, 34796-34804, (2005).
31 Shindo, T. *et al.* ADAMTS-1: a metalloproteinase-disintegrin essential for normal growth, fertility, and organ morphology and function. *J Clin Invest* **105**, 1345-1352, (2000).
32 Le Goff, C. & Cormier-Daire, V. The ADAMTS(L) family and human genetic disorders. *Hum Mol Genet* **20**, R163-167, (2011).
33 Hubmacher, D. & Apte, S. S. Genetic and functional linkage between ADAMTS superfamily proteins and fibrillin-1: a novel mechanism influencing microfibril assembly and function. *Cell Mol Life Sci* **68**, 3137-3148, (2011).
34 Escolano, A. *et al.* Specific calcineurin targeting in macrophages confers resistance to inflammation via MKP-1 and p38. *EMBO J* **33**, 1117-1133, (2014).
35 Chen, X., Lu, H., Rateri, D. L., Cassis, L. A. & Daugherty, A. Conundrum of angiotensin II and TGF-beta interactions in aortic aneurysms. *Curr Opin Pharmacol* **13**, 180-185, (2013).
36 Cook, J. R. *et al.* Dimorphic effects of transforming growth factor-beta signaling during aortic aneurysm progression in mice suggest a combinatorial therapy for Marfan syndrome. *Arterioscler Thromb Vasc Biol* **35**, 911-917, (2015).
37 Guo, D. C. *et al.* Recurrent gain-of-function mutation in PRKG1 causes thoracic aortic aneurysms and acute aortic dissections. *Am J Hum Genet* **93**, 398-404, (2013).
38 Karimi, A. & Milewicz, D. M. Structure of the Elastin-Contractile Units in the Thoracic Aorta and How Genes That Cause Thoracic Aortic Aneurysms and Dissections Disrupt This Structure. *Can J Cardiol* **32**, 26-34, (2016).
39 Kelwick, R., Desanlis, I., Wheeler, G. N. & Edwards, D. R. The ADAMTS (A Disintegrin and Metalloproteinase with Thrombospondin motifs) family. *Genome Biol* **16**, 113, (2015).
40 Dan, H. C. *et al.* Akt-dependent regulation of NF-{kappa}B is controlled by mTOR and Raptor in association with IKK. *Genes Dev* **22**, 1490-1500, (2008).
41 O'Sullivan, S., Medina, C., Ledwidge, M., Radomski, M. W. & Gilmer, J. F. Nitric oxide-matrix metaloproteinase-9 interactions: biological and pharmacological significance--NO and MMP-9 interactions. *Biochim Biophys Acta* **1843**, 603-617, (2014).
42 Van Doren, S. R. Matrix metalloproteinase interactions with collagen and elastin. *Matrix Biol* **44-46**, 224-231, (2015).
43 Segura, A. M. *et al.* Immunohistochemistry of matrix metalloproteinases and their inhibitors in thoracic aortic aneurysms and aortic valves of patients with Marfan's syndrome. *Circulation* **98**, II331-337; discussion II337-338 (1998).
44 Biddinger, A., Rocklin, M., Coselli, J. & Milewicz, D. M. Familial thoracic aortic dilatations and dissections: a case control study. *J Vasc Surg* **25**, 506-511, (1997).
45 Girardi, L. N. & Coselli, J. S. Inflammatory aneurysm of the ascending aorta and aortic arch. *Ann Thorac Surg* **64**, 251-253, (1997).

46 Roth, M., Lemke, P., Bohle, R. M., Klovekorn, W. P. & Bauer, E. P. Inflammatory aneurysm of the ascending thoracic aorta. *J Thorac Cardiovasc Surg* **123**, 822-824, (2002).
47 Gao, Y. *et al.* A disintegrin and metalloproteinase with thrombospondin motif 1 (ADAMTS1) expression increases in acute aortic dissection. *Sci China Life Sci* **59**, 59-67, (2016).
48 Johanning, J. M. *et al.* Nitric oxide in experimental aneurysm formation: early events and consequences of nitric oxide inhibition. *Ann Vasc Surg* **16**, 65-72, (2002).
49 Johanning, J. M., Franklin, D. P., Han, D. C., Carey, D. J. & Elmore, J. R. Inhibition of inducible nitric oxide synthase limits nitric oxide production and experimental aneurysm expansion. *J Vasc Surg* **33**, 579-586, (2001).
50 Kuhlencordt, P. J. *et al.* Accelerated atherosclerosis, aortic aneurysm formation, and ischemic heart disease in apolipoprotein E/endothelial nitric oxide synthase double-knockout mice. *Circulation* **104**, 448-454 (2001).
51 Lee, J. K., Borhani, M., Ennis, T. L., Upchurch, G. R., Jr. & Thompson, R. W. Experimental abdominal aortic aneurysms in mice lacking expression of inducible nitric oxide synthase. *Arterioscler Thromb Vasc Biol* **21**, 1393-1401 (2001).
52 Zhang, J. *et al.* Inducible nitric oxide synthase is present in human abdominal aortic aneurysm and promotes oxidative vascular injury. *J Vasc Surg* **38**, 360-367 (2003).
53 Fukuda, S. *et al.* Prevention of rat cerebral aneurysm formation by inhibition of nitric oxide synthase. *Circulation* **101**, 2532-2538 (2000).
54 Sadamasa, N., Nozaki, K. & Hashimoto, N. Disruption of gene for inducible nitric oxide synthase reduces progression of cerebral aneurysms. *Stroke* **34**, 2980-2984, (2003).
55 Shores, J., Berger, K. R., Murphy, E. A. & Pyeritz, R. E. Progression of aortic dilatation and the benefit of long-term beta-adrenergic blockade in Marfan's syndrome. *N Engl J Med* **330**, 1335-1341, (1994).
56 De Backer, J. *et al.* Marfan Syndrome and Related Heritable Thoracic Aortic Aneurysms and Dissections. *Curr Pharm Des* **21**, 4061-4075 (2015).

FIGURE LEGENDS

Figure 1. Induction of syndromic TAA by Adamts1 deficiency. **(a)** Representative images of Adamts1 immunostaining on aortic sections from the indicated mice (n=3). Scale bar, 20 µm. **(b)** Representative ultrasound images of AR, AsAo and AbAo from mice treated with Ang-II or vehicle (control) for 28 days. Red lines mark the lumen boundary and yellow the lumen diameter. Scale bars, 1mm. **(c)** Maximal diameter (mean±SEM) of the indicated aortic sections from control-treated mice (*Adamts1*$^{+/+}$, n=13; *Adamts1*$^{+/-}$, n=15) and from AngII-treated mice (*Adamts1*$^{+/+}$, n=11; *Adamts1*$^{+/-}$, n=14). Two-way ANOVA, ****p<0.0001 *Adamts1*$^{+/+}$ vs *Adamts1*$^{+/-}$; $^{\#}$p<0.05, $^{\#\#}$p<0.01, $^{\#\#\#}$p<0.001, $^{\#\#\#\#}$p>0.0001, Control vs Ang-II. **(d)** Survival curve of the Ang-II-treated cohort of *Adamts1*$^{+/+}$ and *Adamts1*$^{+/-}$ mice shown in (c). Log-rank (Mantel-Cox) test, *p<0.05. Numbers on charts show the number of live mice / the total number of mice at 28 days. **(e)** Aneurysm incidence in the same cohort. **(f)** End-of-treatment systolic and diastolic BP. Two-way ANOVA, ***p<0.01, ****p<0.001 Adamts1$^{+/+}$ vs *Adamts1*$^{+/-}$; $^{\#\#\#\#}$p<0.0001 Control vs Ang-II. **(g)** Representative H&E staining of sections from 10 *Adamts1*$^{+/+}$ and 7 *Adamts1*$^{+/-}$ insufflated lungs. *indicates progressive distal airspace enlargement. Scale bars, 500 µm (left) and 50 µm (right). **(h)** Representative skeletal PET-CT images of 16-20-week-old *Adamts1*$^{+/+}$ (n=10) and *Adamts1*$^{+/-}$ mice (n=9). Red dotted lines, 1.67 cm; bar, 1 cm. Kyphosis incidence is indicated. **(i)** Anteroposterior and transverse thoracic diameters (mean±SEM) and length quantification of (**j**) cranium and (**k**) humerus, femur and tibia (mean±SEM) of 20 *Adamts1*$^{+/+}$ and 17 *Adamts1*$^{+/-}$ mice. Student's t-test, ns, non-significant; **p<0.01 and ***p<0.001.

Figure 2. *Adamts1* knockdown in the aorta of adult mice causes an aortic disease similar to that induced by *Adamts1* genetic deficiency. Eight-week-old C57BL/6 mice were inoculated through the jugular vein with lentivirus expressing GFP and either *siCtl* or *siAdamts1*. **(a)** Experimental timeline. White triangle, Eco-BP: ultrasound and BP analysis; LVi, lentivirus inoculation; Ang II, Ang-II minipump implantation. **(b)** Representative GFP and Adamts1 immunostaining on AsAo sections. Scale bar, 50 µm. **(c)** Adamts1 immunoblot analysis in aortic samples from mice transduced and treated as indicated. Gapdh expression was used as a loading control. End-of-treatment **(d)** systolic and diastolic BP (mean±SEM) and (**e**) maximal aortic diameter (mean±SEM) in 14 control siCtl, 16 control *siAdamts1*, 13 Ang-II *siCtl*, and 16 Ang-II *siAdamts1* mice. Two-way ANOVA, ***p<0.01, ****p<0.001 *siCtl* vs *siAdamts1*; $^{\#}$p<0.05, $^{\#\#\#}$p<0.001, and $^{\#\#\#\#}$p<0.0001, control vs Ang-II. Results in D-E are pooled data from two independent experiments. **(f)** Images show Masson's trichrome (Masson T.), elastic van Gieson (EVG) and Alcian blue staining. Arrow heads point to elastin breaks. Scale bar, 50 µm. **(g,h)** Quantification of elastin breaks and collagen content in AsAo sections from the mouse cohorts shown in Figures 1 and 2d-2e. Two-way ANOVA, **p<0.01, ***p<0.001, ****p<0.0001 *siCtl* vs *siAdamts1* or *Adamts1*$^{+/+}$ vs *Adamts1*$^{+/-}$; $^{\#\#}$p<0.01, $^{\#\#\#}$p<0.001, $^{\#\#\#\#}$p<0.0001 Control vs Ang-II. **(i)** Representative Tgfβ1, pSmad2 and total Smad2/3 immunohistochemistry of AsAo sections from Control or Ang-II-treated *Adamts1*$^{+/+}$ and *Adamts1*$^{+/-}$ mice (n=3).

Figure 3. *Adamts1* knockdown rapidly induces aortic dilation, hypotension and medial degeneration independently of TGFβ activation. **(a)** Experimental timeline. Eight-week-old C57BL/6 mice were inoculated through the jugular vein with *siCtl* or *siAdamts1* lentivirus and monitored for aortic dilation and BP at the indicated times. (**b**) Adamts1 expression analyzed in aortic extracts by RT-qPCR in 12 *siCtl*, 3 *siAdamts1* for 1,2,3,4,21 days, 10 *siAdamts1* for 7 days and 4 *siAdamts1* for 49 days. mRNA amounts were normalized to *Gapdh* expression (means±SEM). One-way ANOVA, **p<0.01, ***p<0.001, ****p<0.0001 vs *siCtl*. **(c)** Systolic BP; **(d)** elastin breaks in the AsAo; **(e)** maximal diameter of AsAo and AbAo; and (**f**) collagen content of the AsAo (mean±SEM) at the indicated times in mice transduced with *siCtrl* or *siAdamts1* lentivirus. (c,e) Numbers of mice per group were n=12. (d,f) siCtl: n=7; *siAdamts1*: n=6 (day1), n=4 (day2), n=5 (day3, day4, day7), n=3 (day14, day21), n=4 (day 49). (d,f) One-way ANOVA and (c,e) Repeated-measurements two-way ANOVA, *p<0.05, **p<0.01, ***p<0.001, ****p<0.0001 vs *siCtl* at the same time-point. (**g**) Representative zymogram analysis of Mmp2 and Mmp9 activity in aortic extracts prepared 4 days after transduction of mice with *siCtl* or *siAdamts1* (n=3). (**h**) Representative images of Mmp9 (red), Sma (white), and F4/80 immunofluorescence, elastin autofluorescence (green), and DAPI-stained nuclei (blue) in aortic sections from *siCtl* and *siAdamts1* mice (4 days post-inoculation). Atheroma plaques from *Apoe*$^{-/-}$ mice fed a high-fat diet were used as a positive control of F4/80 staining. Bar, 50 µm. (**i**) Experimental scheme. One group of animals received intraperitoneal injection of a neutralizing anti-TGFß antibody 3 days before lentivirus inoculation, and injections were repeated 3 times per week. Another group was treated with losartan by osmotic minipump delivery beginning immediately before lentivirus inoculation. (**j**) Changes in maximal AsAo diameter and end-of-experiment quantification of (**k**) elastin breaks and (**l**) collagen content in aortic sections in the indicated experimental groups (mean±SEM). Numbers of mice per group were 8 siCtrl, 4 siCtrl losartan, 5 *siAdamts1*, 7 *siAdamts1* losartan, and 6 *siAdamts1* anti-TGFβ. (j) Repeated-measurements two-way ANOVA of group means and (k,l) one-way ANOVA, **p<0.001, ***p<0.001, ****p<0.0001 vs si-Ctl; n.s., non-significant. (b,e,h) siCtl

654 results were stable throughout the experimental period, and data are means of readings at 2,

655 4, 7, 14, 21, and 49 days.

656

Figure 4. **The aortopathy induced by *Adamts1* deficiency is mediated by NO. (a)** Experimental design. Eight-week-old C57BL/6 mice were given the NOS inhibitor (L-NAME) in the drinking water, starting 3 days before *siCtl* or *siAdamts1* lentivirus inoculation and continuing for the next 14 days. **(b)** Maximal AsAo and AbAo diameter at the indicated times. **(c, d)** End-of-experiment quantification of (c) elastin breaks and (d) collagen content in aortic sections (mean±SEM; n=5 for each group). **(e)** Quantification of Mmp2 and Mmp9 activity in aortic extracts from *siAdamts1*-transduced mice treated with L-NAME (mean±SEM; n=3 for each group). (b) Repeated-measurements two-way ANOVA of group means, (c-d) two-way ANOVA, and (e) one-way ANOVA; **p<0.01, ****p<0.0001 vs untreated *siCtl*; $^{\#}$p<0.05, $^{\#\#}$p<0.01, $^{\#\#\#\#}$p<0.0001; ns, non-significant. (**f-i**) Eight-week-old *Adamts1*$^{+/+}$ and *Adamts1*$^{+/-}$ mice were treated with L-NAME for 21 days. (**f**) Maximal AsAo and AbAo diameter (mean±SEM) at the indicated time points. **(g, h, i)** End-of-experiment quantification of (g) systolic BP, (h) elastin breaks, and (i) collagen content. Data were acquired from 12 *Adamts1*$^{+/+}$, 13 *Adamts1*$^{+/+}$ L-NAME, 14 *Adamts1*$^{+/-}$, and 12 *Adamts1*$^{+/-}$ L-NAME mice. (f) Repeated-measurements two-way ANOVA, ***p<0.001, ****p<0.0001 vs *Adamts1*$^{+/-}$ L-NAME at each time point. (g-i) Two-way ANOVA, ***p<0.001, ****p<0.0001, *Adamts1*$^{+/+}$ vs *Adamts1*$^{+/-}$; $^{\#}$p<0.05, $^{\#\#}$p<0.01, $^{\#\#\#\#}$p<0.0001 L-NAME vs Control.

Figure 5. Nos2 is a critical mediator of the aortopathy induced by *Adamts1* deficiency. **(a)** Representative images of Nos2 (red) and Sma (white) immunofluorescence (n=4), elastin autofluorescence (green), and DAPI-stained nuclei (blue) in aortic sections from 16-week-old *Nos2*$^{-/-}$, *Adamts1*$^{+/+}$, and *Adamts1*$^{+/-}$ mice and from *siCtl* or *siAdamts1* mice (4 days post-inoculation). Bar, 50 µm**. (b)** Experimental design. Eight-week-old *Nos2*$^{-/-}$ and wt mice were inoculated with siCtl and *siAdamts1* lentivirus and monitored for aortic dilation and BP. **(c)** Maximal AsAo diameter (mean±SEM) in 6 wt siCtl, 9 wt *siAdamts1*, 4 *Nos2*$^{-/-}$ siCtl, and 7 *Nos2*$^{-/-}$ *siAdamts1* mice at the indicated time points. End-of-experiment quantification of (**d**) elastin breaks and (**e**) collagen content in the same mouse cohort. **(f)** Systolic BP (mean±SEM) at the indicated time points in the same mouse cohort. (c,f) Repeated-measurements two-way ANOVA of group means; ****p<0.0001 vs *Nos2*$^{-/-}$ *siAdamts1*; ns, non-significant. (d,e) Two-way ANOVA; **p<0.01 vs wt *siCtl*; ns, non-significant. **(g)** Representative images (n=3) of NO production (red), elastin autofluorescence (green) and DAPI-stained nuclei (blue) in unfixed aortic tissue sections from *siCtl*, *siAdamts1*, and *Nos2*$^{-/-}$ *siAdamts1* mice (14 days post-inoculation) and from 10-week-old *Adamts1*$^{+/+}$ and *Adamts1*$^{+/-}$ mice. Bar, 50 µm. (**h**) Representative immunoblot analysis of the indicated proteins and phosphorylated residues in aortic extracts of *siCtl* and *siAdamts1* mice. (**i-l**) Eight-week-old *Adamts1*$^{+/+}$ and *Adamts1*$^{+/-}$ mice received 4 daily intraperitoneal injections of the mTOR/Akt inhibitor AZD8055 or vehicle. Numbers of mice per group were 5 control *Adamts1*$^{+/+}$, 6 treated *Adamts1*$^{+/+}$, 4 control *Adamts1*$^{+/-}$, and 7 treated *Adamts1*$^{+/-}$. **(i)** Maximal AsAo diameter (mean±SEM) at the indicated times. **(j)** End-of-experiment systolic BP. **(k)** RT-qPCR analysis of *Nos2* mRNA in aortic extracts from the indicated mice. **(l)** Representative images of NO production (red), elastin autofluorescence (green), and DAPI-stained nuclei (blue) in unfixed aortic tissue sections from the indicated mice. Bar, 50 µm. (i) Repeated-measurements two-way ANOVA and (k) two-way ANOVA; ****p<0.0001 vs untreated *Adamts1*$^{+/-}$.

Figure 6. Adamts1 and NO play a critical role in Marfan syndrome. (a) Representative images (n=3) of NO production (red), Nos2 immunofluorescence (red), elastin autofluorescence (green), and DAPI-stained nuclei (blue) in aortic sections of 16-week-old wt and *Fbn1*$^{C1039G/+}$ mice. **(b)** Representative Adamts1 immunohistochemistry in aortic sections from wt and *Fbn1*$^{C1039G/+}$ mice and immunoblot analysis of Adamts1 in aortic extracts. IgG staining serves as a negative control. Bar, 20 µm. **(c)** RT-qPCR analysis of *Adamts1* mRNA in aortic extracts from 6 wt and 3 *Fbn1*$^{C1039G/+}$ mice. **(d)** Representative medial layer images of ADAMTS1 immunofluorescence (red; n=9) and NOS2 immunofluorescence (red; n=6). Elastin autofluorescence (green) and DAPI-stained nuclei (blue) are also shown. Bar, 25 µm. (**e**) ADAMTS1-positive area in immunohistochemistry-stained sections of 5 control donors and 9 MFS patients. (**f**) NOS2-positive area in sections from 5 control donors and 8 MFS patients. Data in e and f are means ±SEM. Student's t-test; *p<0.05, ***p<0.001. (**g-i**) Twelve-week-old *Adamts1*$^{+/-}$ and *Fbn1*$^{+/C1039G}$ mice and corresponding wt littermates were given 1400W in the drinking water for 16 weeks. **(g)** Maximal AsAo diameter at the indicated times. Data are means ±SEM (n=4); repeated-measurements two-way ANOVA of group means: ****p<0.0001 vs *Adamts1*$^{+/-}$ 1400W or *Fbn1*$^{+/C1039G}$ 1400W; ns, non-significant. **(h)** End-of-experiment systolic BP. Data are means ±SEM (n=4); two-way ANOVA: *p<0.05, ***p<0.001 vs wt Control; $^{\#}$p<0.05, $^{\#\#}$p<0.01 vs *Adamts1*$^{+/+}$ 1400W or *Fbn1*$^{+/+}$ 1400W. **(i)** Representative images of EVG staining in aortic sections from the same group of mice. Bar, 50 µm. (**j-k**) Thirty-six-week-old *Fbn1*$^{+/C1039G}$ mice and wt littermates were given 1400W in the drinking water for 21 days. Numbers of mice per group were 5 control or treated wt; 7 control *Fbn1*$^{+/C1039G}$ and 6 treated *Fbn1*$^{+/C1039G}$. **(j)** Maximal AsAo diameter at the indicated times. Data are means ±SEM; repeated-measurements two-way ANOVA of group means: ***p<0.001 vs *Fbn1*$^{+/C1039G}$ 1400W; ns, non-significant. **(k)** End-of-experiment systolic BP. Data are means ±SEM; two-way ANOVA: *p<0.05 vs Control wt; $^{\#}$p<0.05 vs treated wt. (**l**) Model depicting the contribution of NO and NOS2 to the aortic phenotype in Marfan syndrome and the related aortopathy induced by *Adamts*1 deficiency.

Methods

Animal Procedures

Animal procedures were approved by the CNIC Ethics Committee and by the Madrid regional authorities (Ref. PROEX 80/16), and conformed with EU Directive 2010/63EU and Recommendation 2007/526/EC regarding the protection of animals used for experimental and other scientific purposes, enforced in Spanish law under Real Decreto 1201/2005. *Adamts1*$^{+/-}$ mice were obtained from the European Mouse Mutant Archive [(EM:02291) B6;129P2-Adamts1<tm1Dgen>/H] and carried a LacZ-Neo cassette to replace a genomic sequence (c7784) between exon1 and 2 in the *Adamts1* target allele. *Fbn1*$^{C1039G/+}$ mice[57], harboring a mutation in the Fbn1 gene, and *Nos2*$^{-/-}$ mice[58] were obtained from Jackson Laboratories (JAX mice stock # 012885 and 007072, respectively). These 3 strains had been previously backcrossed to C57BL/6 for more than nine generations. All mice were genotyped by PCR of tail samples using the following primers: *Adamts1* mice (5´-GCCATCGGGGTCAGCTTTTCAAATG-3´, 5´-GGGCCAGCTCATTCCTCCCACTCAT/ GGTTGTAGTTTCGCGCTGAGTTTTG-3´); *Nos2*$^{-/-}$ mice (5' ACATGCAGAATGAGTACCGG 3'; 5' TCAACATCTCCTGGTGGAAC 3´, 5' AATATGCGAAGTGGACCTCG 3'); *Fbn1*$^{C1039G/+}$ mice (5´CTC ATC ATT TTT GGC CAG TTG 3´, 5´GCA CTT GAT GCA CAT TCA CA 3´). Wild-type littermates were used as controls unless otherwise specified. Mice were treated with Ang-II (Sigma-Aldrich) at 1 μg/kg/min or with losartan (Sigma Aldrich) at 10mg/kg/day using subcutaneous osmotic minipumps (Alzet Corp). The monoclonal pan-antibody against TGFβ1, 2, 3 clone 1D11 (BioXcell) was injected intraperitoneally 3 times per week at 10mg/kg. Nω-Nitro-L-arginine methyl ester hydrochloride (L-NAME, Sigma-Aldrich, 0.5 g/l) and 1400W (Tebu-bio, 0.1 g/l) were supplied in drinking water for the indicated periods, plus an additional 3 days before lentivirus inoculation. AZD8055 (Selleck Chem, S1555) was dissolved in 8% DMSO/corn oil and administered daily i.p. (20mg/kg/day).

Blood Pressure Measurements and In Vivo Imaging

Arterial blood pressure (BP) was measured in mouse tails using the automated BP-2000 Blood Pressure Analysis System (Visitech Systems, Apex, NC, USA). In brief, mice were trained for BP measurements every day for one week. After training, BP was measured one day before treatment or before lentiviral infection to determine the baseline BP values in each mouse cohort. Measurements were repeated several times during experiments. BP measurements were recorded in mice located in a tail-cuff restrainer over a warmed surface (37ºC). Fifteen consecutive systolic and diastolic BP measurements were made, and the last ten readings per mouse were recorded and averaged.

For *in vivo* ultrasound images, the aortic diameter was monitored in isoflurane-anesthetized mice (2% isoflurane) by high-frequency ultrasound with a VEVO 2100 echography device (VisualSonics, Toronto, Canada) with 30 micron resolution. Maximal internal diameters of aortic images were measured using VEVO 2100 software, version 1.5.0. All recordings were made by a cardiologist and a technician who were blinded to animal genotype and treatment. Measurements were taken before lentivirus administration or the corresponding treatments to determine the baseline diameters, and measurements were repeated several times during the experiment. In the indicated cases, the maximum external diameter of the AsAo was measured after sacrifice using a digital caliper (Ratio 6369H15).

The whole skeleton was imaged in anesthetized mice (1.5-2% isofluorane) using an X-Ray CT system integrated in a nano PET-CT scanner (Mediso Medical Imaging Systems, Budapest). Images were acquired at 55Kv, 500mA/sec, 360 frames per Rx rotation, and pitch = 1. Skeletal 3D reconstruction was performed with Medis software (Medis, The Netherlands).

Cell Procedures

Primary mouse vascular smooth muscle cells (VSMC) were isolated and grown as described[20]. All experiments were performed during passages 3-7. VSMCs were infected at a multiplicity of infection = 3 over 5h. The medium was then replaced with fresh DMEM supplemented with 10%FBS, and cells were cultured for 3 more days, serum-starved for 48h,

and then stimulated with Ang-II for 6h for protein assays or 4h for mRNA expression analysis. HEK-293T and Jurkat cell lines were purchased from ATCC. All cells were *mycoplasma*-negative.

siRNA-encoding Lentivirus Production and Infection.

Lentiviruses expressing GFP and siRNA targeting mouse *Adamts1* mRNA were purchased from ABM-GOOD. siRNA sequences were as follows: #siRNA27 (GGAAAGAATCCGCAGCTTTAGTCCACTCA); #siRNA57 (ACCGCCAGTGTCAGTTTACATTCGGAGAG); #siRNA69 (CTTCCGAATGTGCAAAGGAAGTGAAGCCA). siCtl (GGGTGAACTCACGTCAGAA) was used as a control. Pseudo-typed lentiviruses were produced by transient calcium phosphate transfection of HEK-293T cells. Supernatant containing the lentiviral particles was collected 48h after removal of the calcium phosphate precipitate, and ultracentrifuged for 2h at 26,000rpm (Ultraclear Tubes, SW28 rotor and Optima L-100 XP Ultracentrifuge; Beckman). Viruses were suspended in cold sterile PBS solution and titrated by transduction of Jurkat cells for 48h. Transduction efficiency (GFP-expressing cells) and cell death (propidium iodide staining) were quantified by flow cytometry.

For *in vivo* transduction experiments, animals were anesthetized (ketamine/xilacine) and a small incision was made to expose the right jugular vein[20]. Virus solution (100 µl, 10^9 particles/ml in PBS) was inoculated directly into the right jugular vein 3 weeks before Ang-II mini-pump implantation or one day before monitoring of aortic dilation. Transduction efficiency was analyzed in aortic samples by immunohistochemistry for GFP and Adamts1.

Aortic Histology

After sacrifice by CO_2 inhalation, mouse aortas were perfused with saline, isolated, and fixed in 4% paraformaldehyde overnight at 4ºC. Paraffin cross sections (5-µm) from fixed aortas were stained with Masson's trichrome (Masson), alcian blue, or Verhoeff elastic–van Gieson (EVG) or were used for immunohistochemistry or immunofluorescence. Deparaffinized sections were rehydrated, boiled to retrieve antigens (10mM citrate buffer, pH6), and blocked for 45min with 10% goat serum plus 2% BSA in PBS. Samples were

812 incubated with the following antibodies for immunohistochemistry or immunofluorescence:
813 Rabbit anti-Adamts1 (1/100, sc-25581, Santa Cruz), rabbit anti-GFP (1/100, A11122,
814 Invitrogen), rabbit anti-pSMAD2 (1/50, 3108, Cell Signaling for IHC; 1/20, 566415,
815 Calbiochem, for IF), rabbit anti-SMAD2/3 (sc-8332 1/100 Santa Cruz), rabbit anti-TGF β 1
816 (1/100; Abcam ab92486), rabbit anti-NOS2 (1/100, sc-650, Santa Cruz, for mice; 482728,
817 Millipore, for human), monoclonal anti-SMA (1/500, C6198, Sigma), rat anti-F4/80 (1/50,
818 MF48015, Invitrogen), and rabbit anti-MMP9 (1/100, ab38898, Abcam). Specificity was
819 determined by substituting primary antibody with unrelated IgG (Santa Cruz). For
820 immunohistochemistry, color was developed with DAB (Vector Laboratories), and sections
821 were counterstained with hematoxylin and mounted in DPX (Fluka). Images were acquired
822 under a Leica DM2500 microscope with 20x, 40x, or 63xHCX PL Fluotar objective lenses
823 and Leica Application Suite V3.5.0 acquisition software. For immunofluorescence, secondary
824 antibodies were AlexaFluor546-conjugated goat anti-rabbit and AlexaFluor647-conjugated
825 goat anti-rabbit (BD Pharmigen). Sections were mounted with DAPI in Citifluor AF4 mounting
826 medium (Aname). Images were acquired at 1024x1024 pixels, 8bits, using a Leica SP5
827 confocal microscope with 20x or 40x oil immersion objectives.
828 Collagen fibers in aortic sections were stained with a Masson-Goldner's trichrome
829 staining kit (Merck), and elastic fibers were stained with a modified Verhoeff Van Gieson
830 elastin stain kit (Sigma-Aldrich). Images were acquired under a Leica DM2500 microscope
831 with 20x, 40x or 63xHCX PL Fluotar objective lenses and Leica Application Suite V3.5.0
832 acquisition software and processed for presentation with Photoshop and Illustrator (Adobe)
833 according to the guidelines of this Journal. Images were then analyzed with MetaMorph 6.1
834 software (Universal Imaging Corp., Downingtown, PA). Collagen was quantified by
835 thresholding the green signal using the hue-saturation-intensity color model and determining
836 the percentage of stained area in the medial layer of 2 non-consecutive full aortic cross
837 sections per mouse, employing 4-16 mice per experiment. The mean percentage was
838 calculated. Elastic lamina breaks, defined as interruptions in the elastic fibers, were counted
839 in 6 non-consecutive, full aortic sections per mouse, employing 4-16 mice per experiment, and

the mean number of breaks was calculated. The exact number of mice per group is indicated in the figure legends.

Immunoblot Analysis

Mouse aortic samples were isolated, frozen in liquid nitrogen and then homogenized (MagNA lyzer, Roche). Protein extracts were obtained by lysis in ice-cold RIPA buffer (50mM NaCl, 50mM Tris HCl pH8, 1% NP40, 0.1% SDS, 0.5% sodium deoxycolate) completed with protease, phosphatase, and kinase inhibitors. For VSMCs, cells were infected and then stimulated with AngII, washed with ice-cold PBS, and lysed in RIPA buffer.

Proteins were separated under reducing conditions on SDS-polyacrylamide gels and transferred to nitrocellulose membranes. Proteins were detected with the following primary antibodies: rabbit anti-Adamts1 (1/1000; sc-25581 Santa Cruz), anti-Nos2 (1/1000, sc-650 Santa Cruz), anti-p-AKT-S473 (1/1000, #9271 Cell Signaling), anti AKT (1/1000, #9272 Cell Signaling), anti-p-p65(1/500, #3033 Cell Signaling), and anti-p65 (1/1000, #8242 Cell Signaling); mouse monoclonal anti-alpha tubulin (1/40,000; T 6074 Sigma-Aldrich) and anti-GAPDH (1/10,000; ab8245 Abcam). Bound antibodies were detected with enhanced chemiluminescence (ECL) detection reagent (Millipore).

RT and Quantitative PCR

Aortas were extracted after perfusion with 5ml saline solution, and the adventitia layer was discarded. Frozen tissue was homogenized using a mortar and an automatic bead homogenizer (MagNA Lyzer, Roche). Total RNA was isolated with TRIZOL (Life Technologies). Total RNA (2 µg) was reverse transcribed at 37ºC for 50 min in a 20ul reaction mix containing 200U Moloney murine leukemia virus (MMLV) reverse transcriptase (Life Technologies), 100ng random primers, and 40U RNase Inhibitor (Life Technologies). Real-time quantitative RT-PCR was performed with the following PCR primers: Adamts1 (ACACTGGCGGTTGGCATCGT, GCCAGCCCTGGTCACCTTGC), Tgfß1 (CGCCATCTATGAGAAAACC, GTAACGCCAGGAATTGT), Ctgf (GTGCCAGAACGCACACTG, CCCCGGTTACACTCCAAA), Col1a1

867 (GCTCCTCTTAGGGGCCACT, CCACGTCTCACCATTGGGG), Pai-1 (GCCAGATTT
868 ATCATCAATGACTGGG, GGAGAGGTGCACATCTTTCTC AAAG), Nos3
869 (GTTTGTCTGCGGCGATGTC, CATGCCGCCCTCTGTTG), *Nos2*
870 (CAGCTGGGCTGTACAAACCTT, CATTGGAAGTGAAGCGTTTCG). qPCR reactions were
871 performed in triplicate with SYBR-master mix (Applied Biosystems) according to the
872 manufacturer's guidelines. To examine probe specificity, we conducted a post-amplification
873 melting-curve analysis. For each reaction, only one Tm peak was produced. The amount of
874 target mRNA in samples was estimated by the $2^{-\Delta CT}$ relative quantification method, using
875 *GAPDH* for normalization. Fold ratios were calculated relative to control animals.
876 **Nitric Oxide Staining and Nitrite and Nitrate Quantification**
877 NO was stained in unfixed fresh aortic sections with DAF-FM Diacetate and in VSMCs
878 with DAR-4M (Molecular Probes). Samples were incubated with 10µmol/L DAF-FM Diacetate
879 reagent for 1 hour at RT and mounted in 10% glycerol in PBS. Images were acquired with a
880 Leica SP5 microscope. Nitrites and Nitrates (total NOx) were measured in conditioned
881 medium from transduced VSMCs after 24 hours using a nitric oxide quantitation kit (Active
882 Motif).
883
884 **Zymography**
885 Aortic extracts were prepared from whole aortas as described for immunoblot assays,
886 but in the absence of DTT. Extracts (15µg) were fractioned under nonreducing conditions on
887 SDS-polyacrylamide gels containing 1% gelatin. Gels were washed three times in 2.5%
888 Triton x-100 for 30 min at room temperature, incubated overnight at 37ºC in 50mM Tris-HCl
889 pH 7.5, 10mM $CaCl_2$, and 200mM NaCl, and stained with Coomasie Blue. The areas of
890 gelatinolytic or MMP activity were visualized as transparent bands. Images were analyzed
891 with Quantity One software (Bio-Rad).
892 **Human Samples**
893 The study was approved by the Ethics and Clinical Research Committee of Cantabria
894 (ref.: 27/2013) and by the Ethics committee of Ghent University Hospital (B65020111160).

Control ascending aorta was obtained anonymously from multiorgan transplant donors after written informed consent was obtained from their families. During preparation of the heart for transplantation, excess ascending aortic tissue was harvested for the study. Samples from Marfan syndrome patients were obtained during elective or emergency aortic root surgery for aortic root aneurysm/dissection. Patient clinical data were retrieved while maintaining anonymity. Tissues were immediately fixed, kept at room temperature for 48 hours, and included in paraffin.

Statistical Analysis

Graphpad Prism software 6.01 was used for the analysis. The aortic diameter data are presented as box and whiskers plots, with 75th and 25th percentiles; bars represent maximal and minimal values. Differences were analyzed by one-way, two-way, or repeated-measurements two-way analysis of variance (ANOVA) and Tukey's post-hoc test or Newman's post-hoc test (experiments with ≥3 groups), as appropriate. For survival curves, differences were analyzed with the Log-rank (Mantel-Cox) test. Statistical significance was assigned at *p<0.05, **p<0.01, ***p<0.001, and ****p<0.0001.

Sample size was chosen empirically according to previous experience in the calculation of experimental variability; no statistical method was used to predetermine sample size, and no data were excluded. The numbers of animals used are described in the corresponding figure legends. All experiments were carried out with at least three biological replicates. Experimental groups were balanced in terms of animal age, sex and weight. Animals were genotyped before experiments and caged together and treated in the same way. Appropriate tests were chosen according to the data distribution. Variance was comparable between groups throughout the manuscript. Investigators were blinded to the group allocation in the experiments included in Supplementary Figure 8b. For the rest of experiments, no randomization was used to allocate animals to experimental groups and investigators were not blinded to the group allocation during experiments or outcome assessments.

57 Judge, D. P. et al. Evidence for a critical contribution of haploinsufficiency in the complex pathogenesis of Marfan syndrome. J Clin Invest 114, 172-181, (2004).
58 Laubach, V. E., Shesely, E. G., Smithies, O. & Sherman, P. A. Mice lacking inducible nitric oxide synthase are not resistant to lipopolysaccharide-induced death. Proc Natl Acad Sci U S A 92, 10688-10692 (1995).

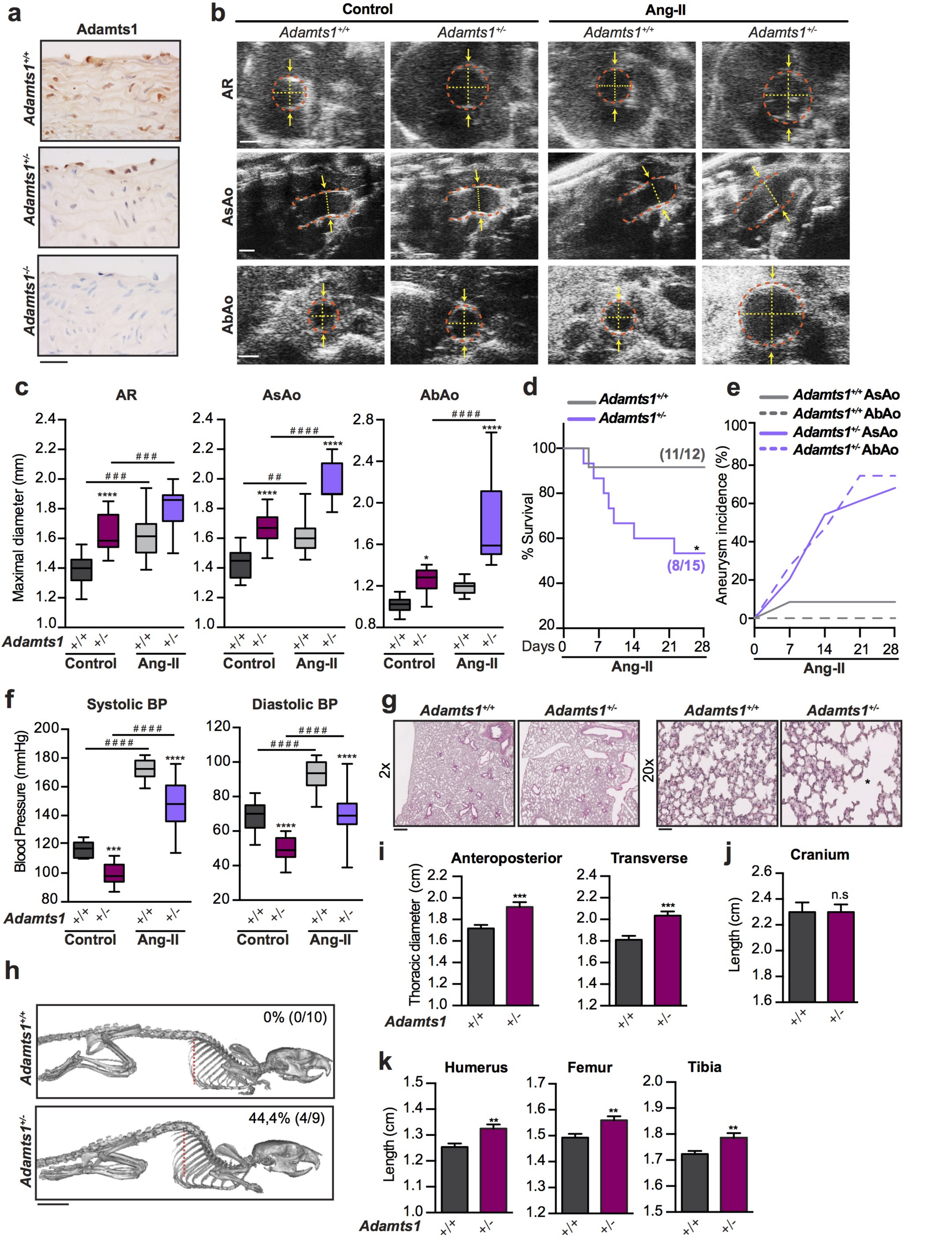
a
Adamts1
Adamts1+/+
Adamts1+/-
Adamts1-/-
b
Control
Ang-II
Adamts1+/+
Adamts1+/-
AR
AsAo
AbAo
c
AR
AsAo
AbAo
Maximal diameter (mm)
Adamts1
Control
Ang-II
d
Adamts1+/+
Adamts1+/-
% Survival
Days
(11/12)
(8/15)
e
Adamts1+/+ AsAo
Adamts1+/+ AbAo
Adamts1+/- AsAo
Adamts1+/- AbAo
Aneurysm incidence (%)
f
Systolic BP
Diastolic BP
Blood Pressure (mmHg)
g
2x
20x
h
0% (0/10)
44,4% (4/9)
i
Anteroposterior
Transverse
Thoracic diameter (cm)
j
Cranium
Length (cm)
n.s
k
Humerus
Femur
Tibia
Length (cm)

Figure1

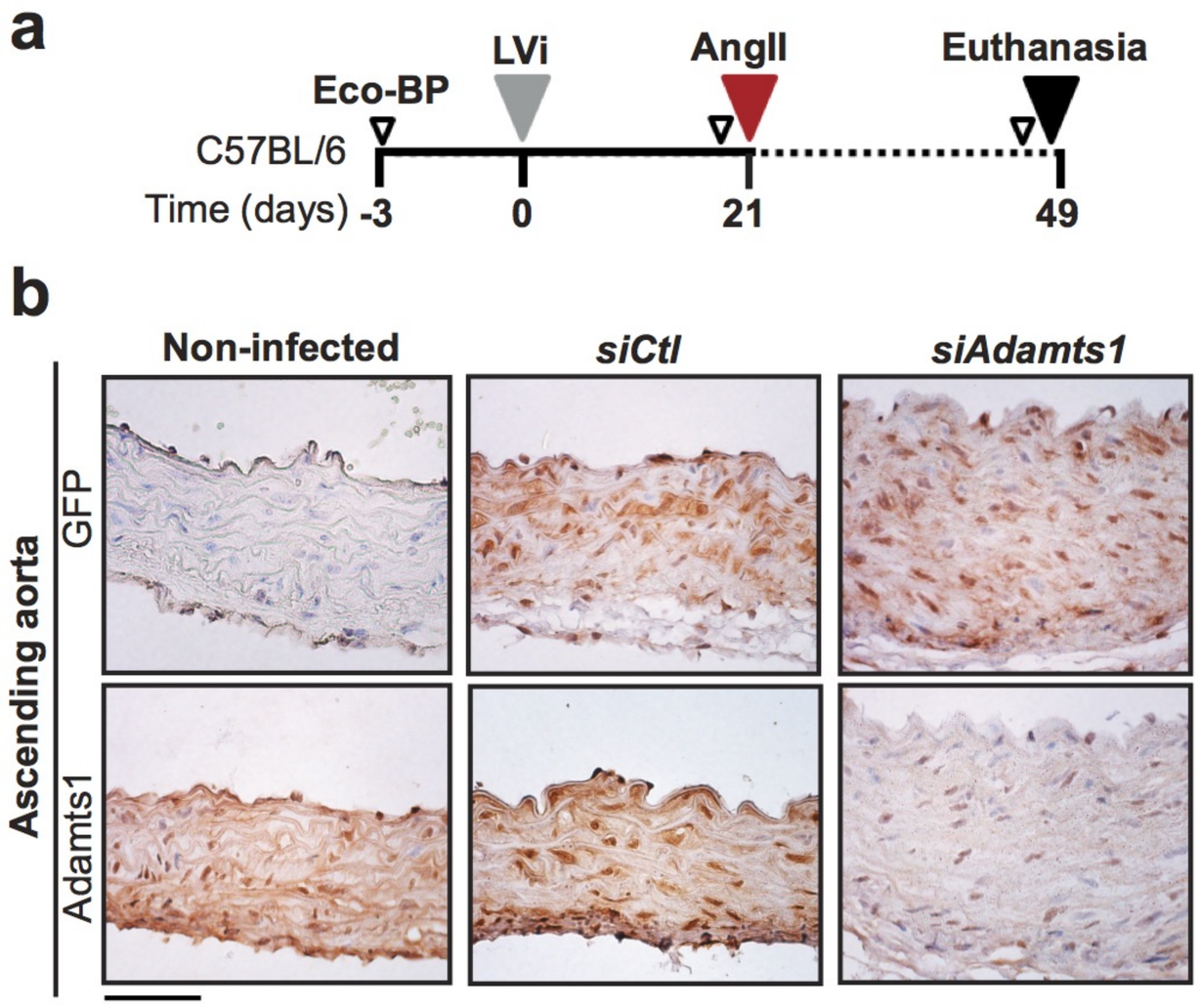
a
Eco-BP
LVi
AngII
Euthanasia
C57BL/6
Time (days) -3
0
21
49
b
Non-infected
siCtl
siAdamts1
Ascending aorta
GFP
Adamts1

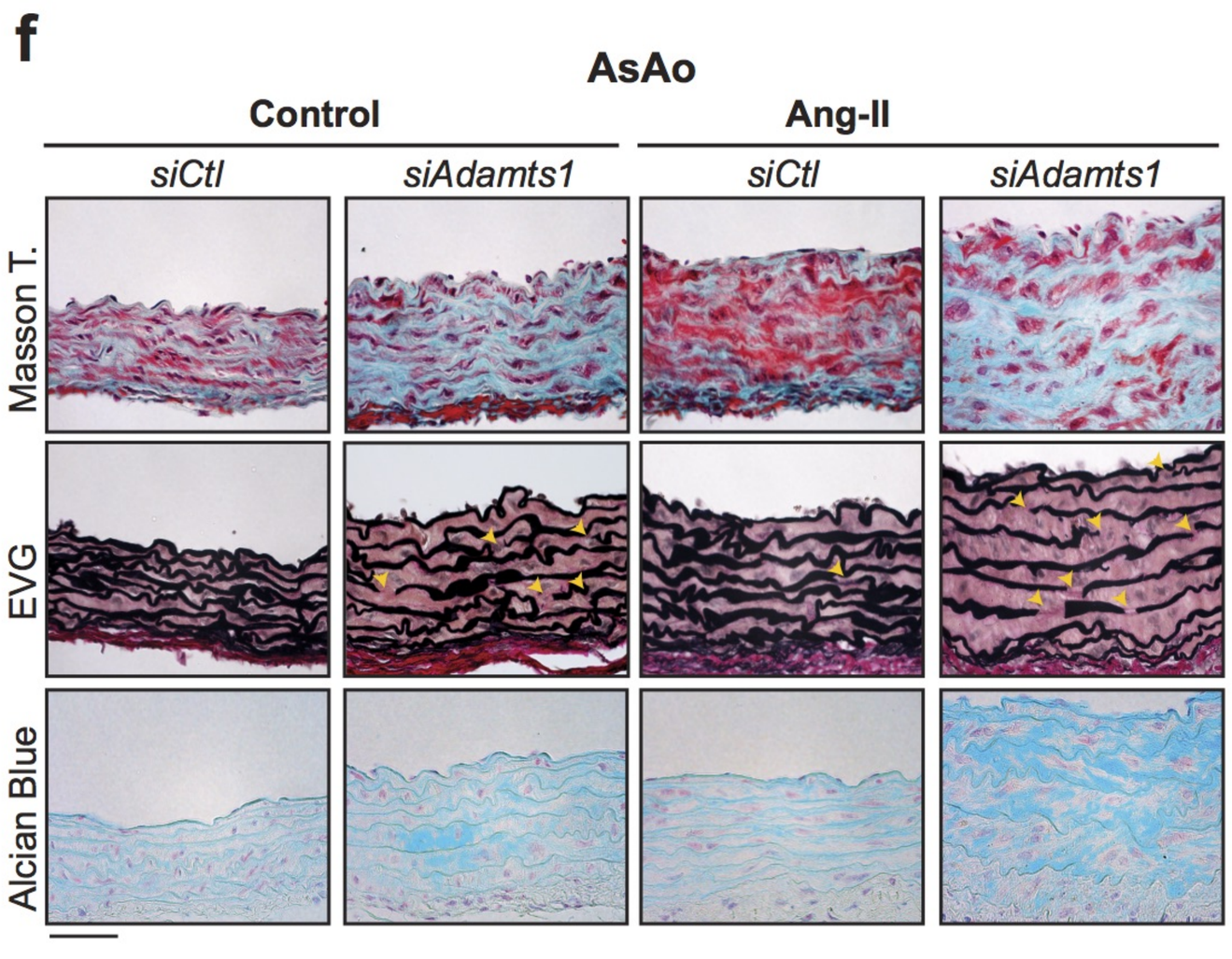
f
AsAo
Control
Ang-II
siCtl
siAdamts1
siCtl
siAdamts1
Masson T.
EVG
Alcian Blue

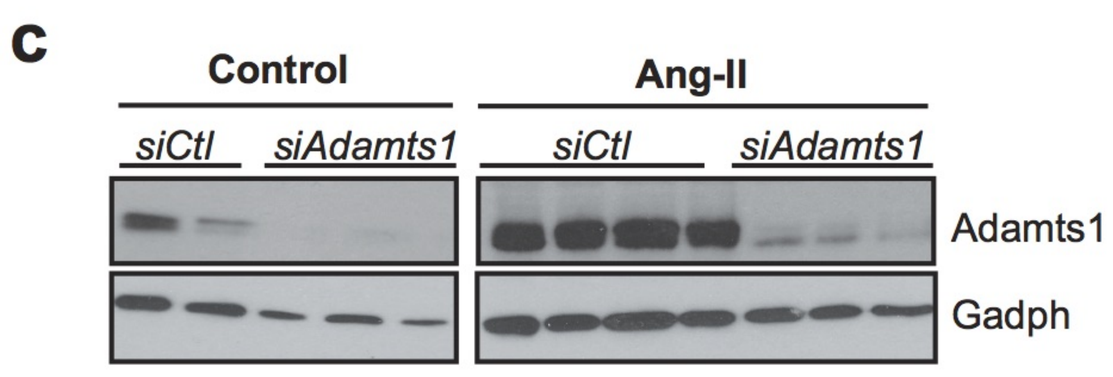
c
Control
Ang-II
siCtl
siAdamts1
siCtl
siAdamts1
Adamts1
Gadph

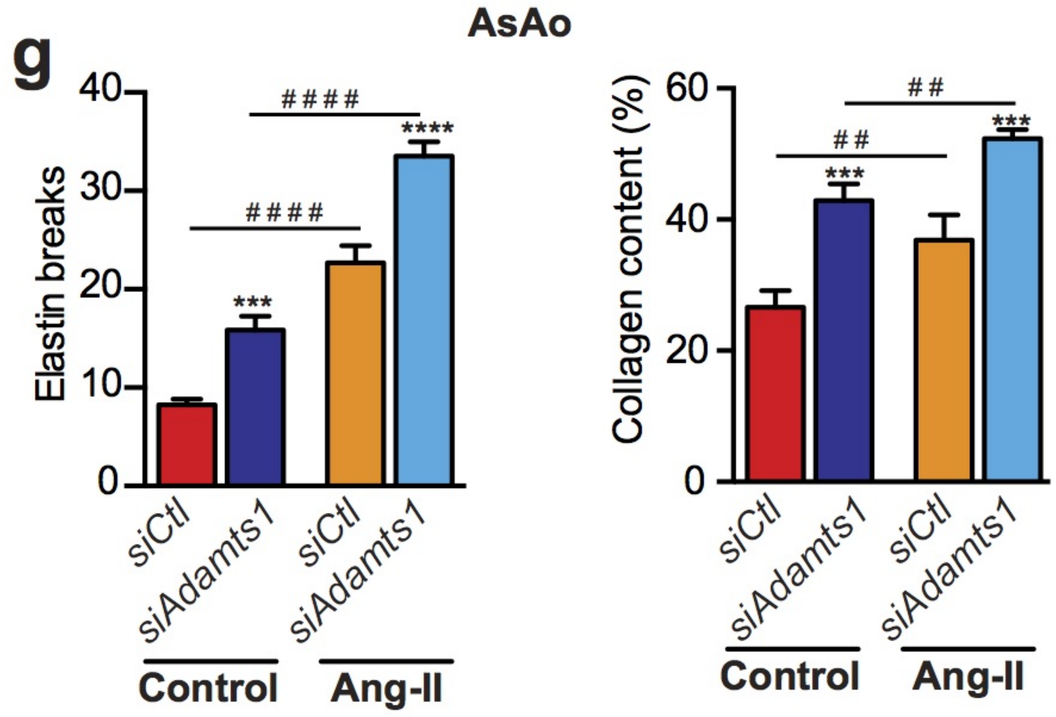
g
AsAo
Elastin breaks
Collagen content (%)
siCtl
siAdamts1
siCtl
siAdamts1
Control
Ang-II

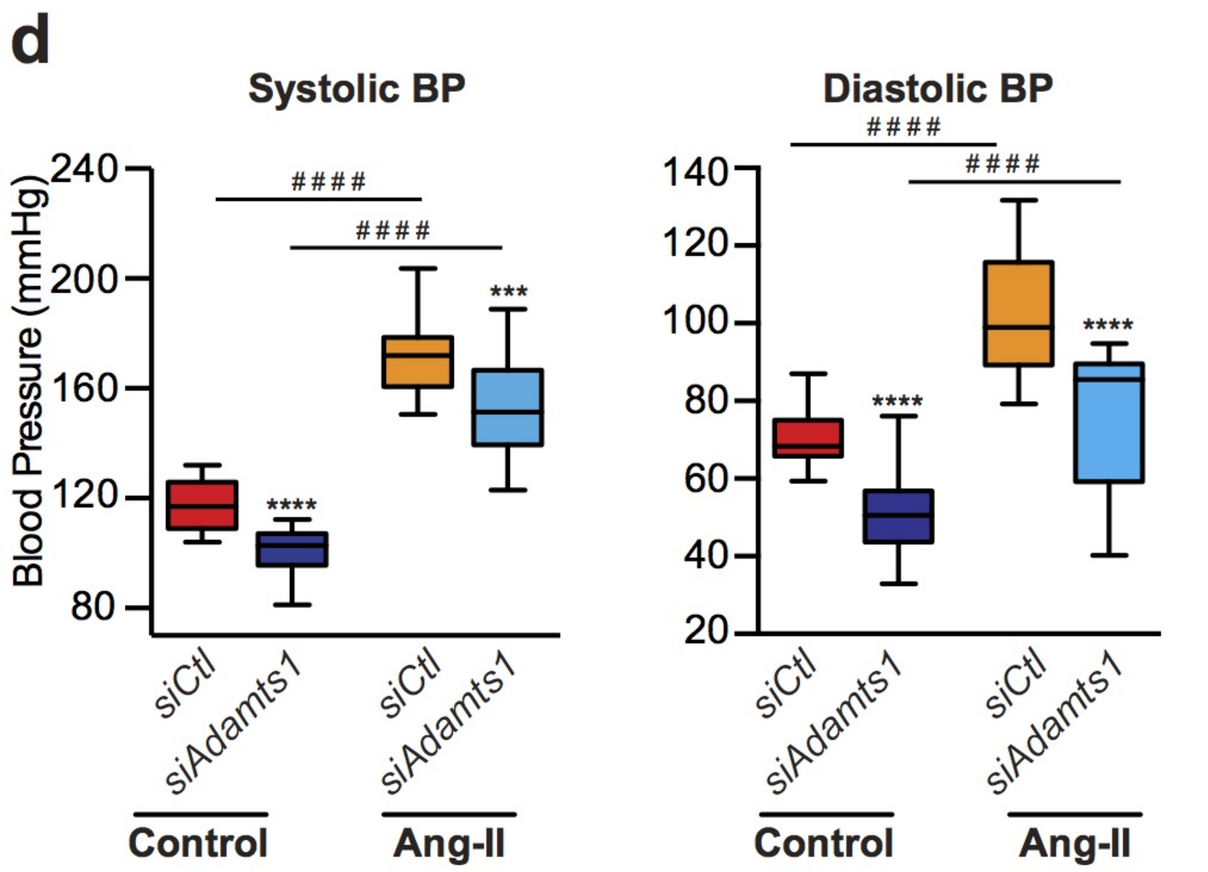
d
Systolic BP
Diastolic BP
Blood Pressure (mmHg)
siCtl
siAdamts1
siCtl
siAdamts1
Control
Ang-II

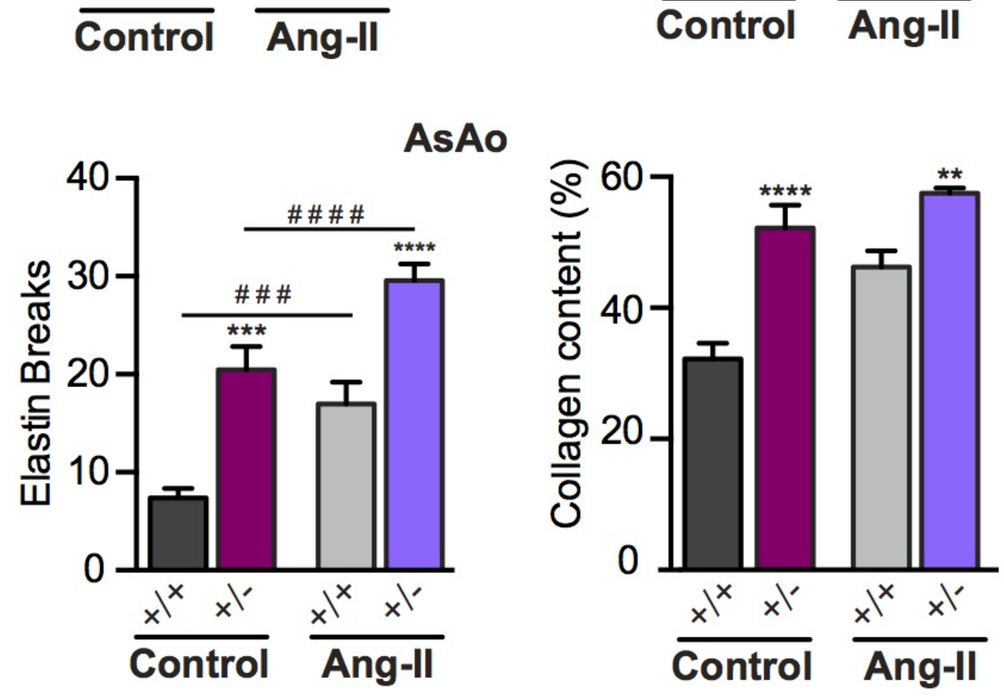
h
AsAo
Elastin Breaks
Collagen content (%)
+/+
+/-
+/+
+/-
Control
Ang-II

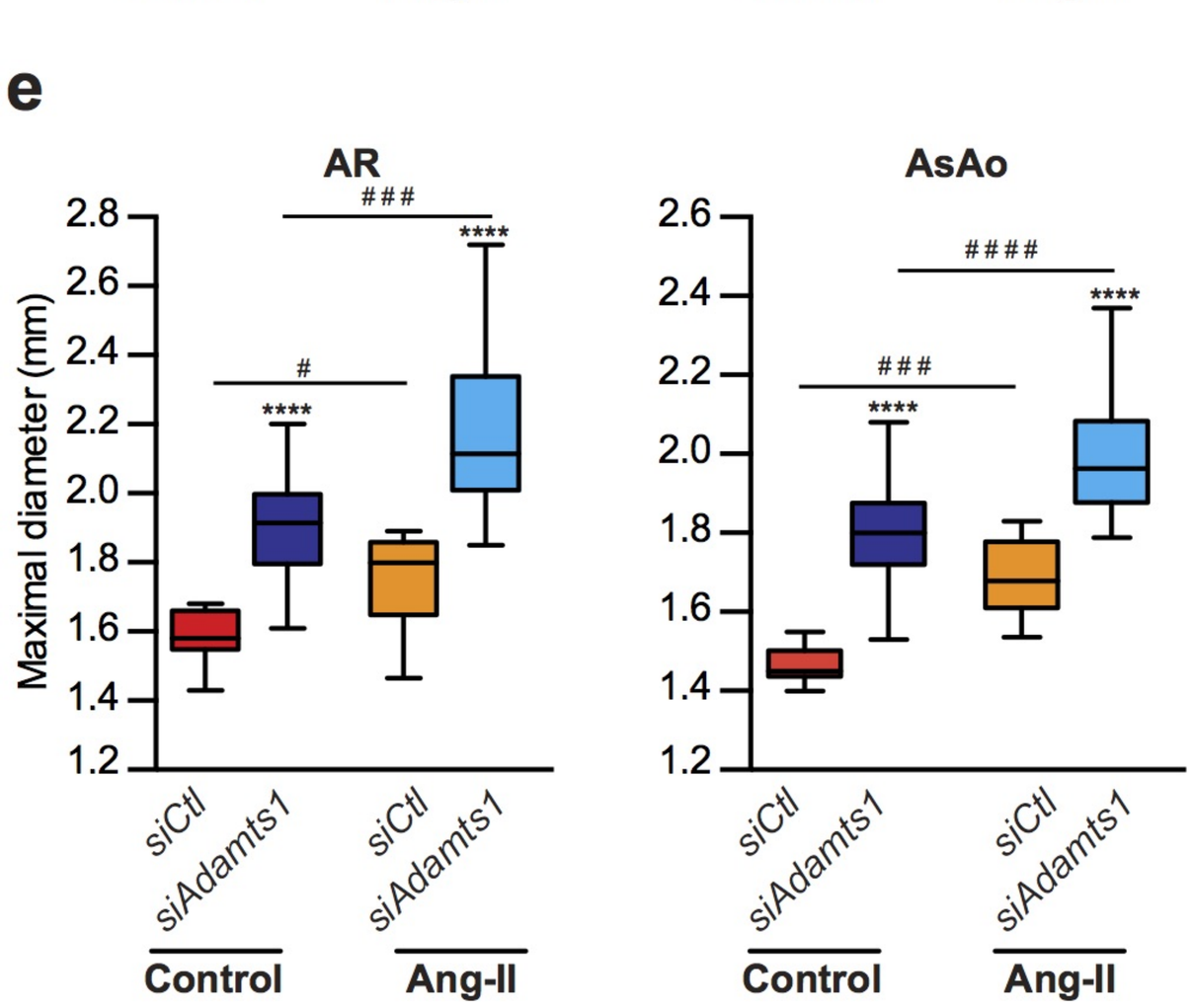
e
AR
AsAo
Maximal diameter (mm)
siCtl
siAdamts1
siCtl
siAdamts1
Control
Ang-II

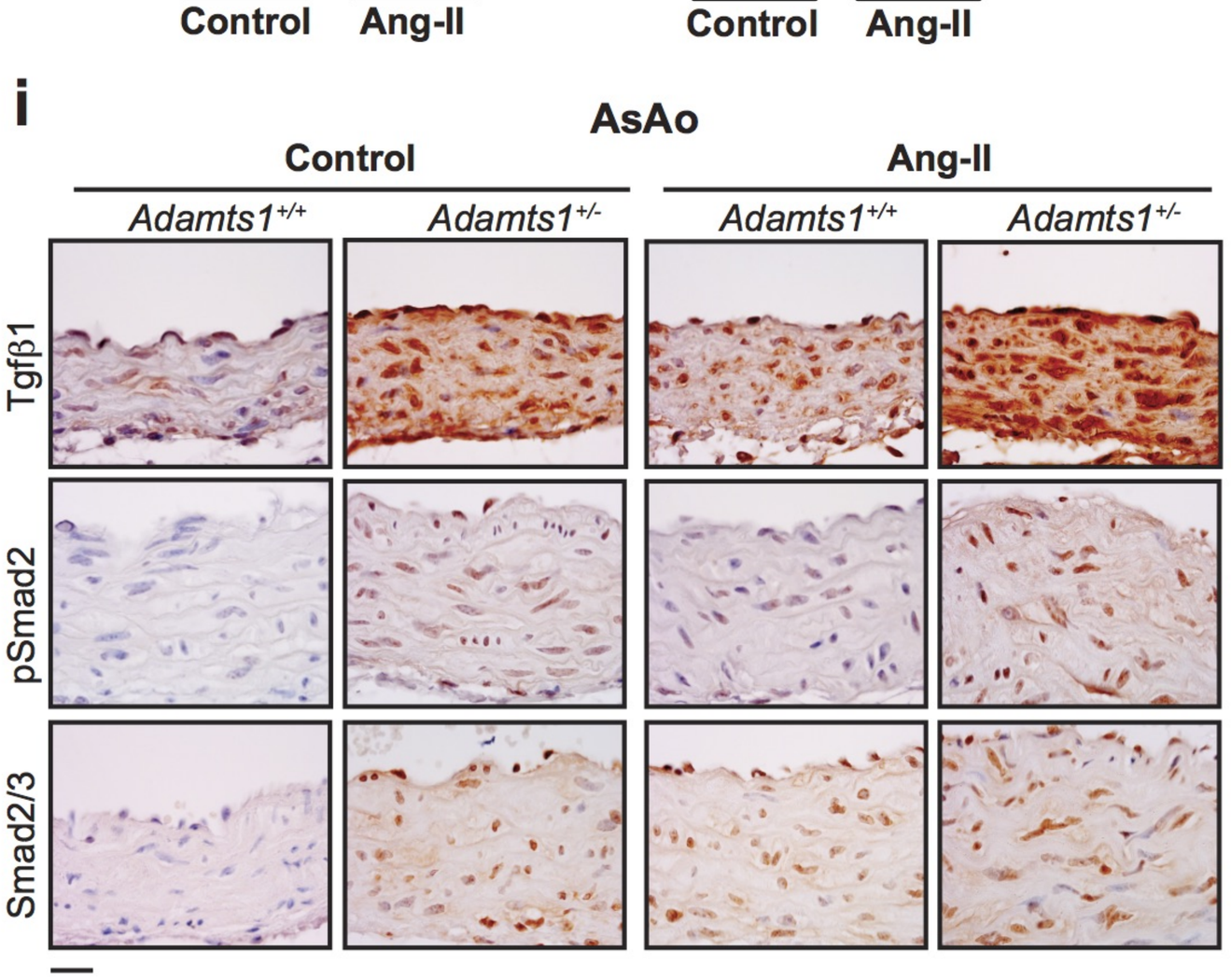
i
AsAo
Control
Ang-II
Adamts1+/+
Adamts1+/-
Adamts1+/+
Adamts1+/-
Tgfβ1
pSmad2
Smad2/3

Figure 2

Figure 3

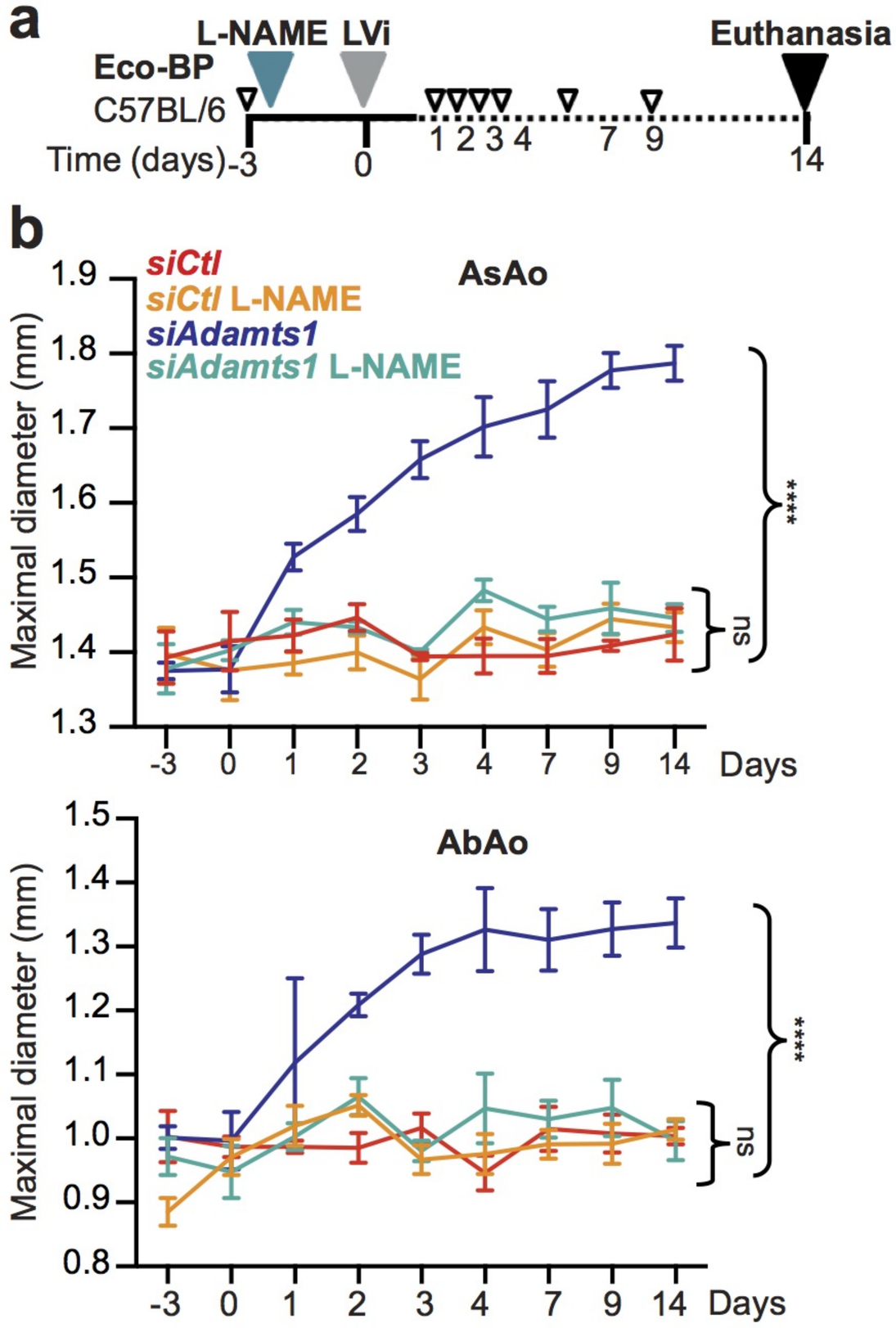
a
L-NAME
LVi
Euthanasia
Eco-BP
C57BL/6
Time (days)
-3
0
1 2 3 4
7
9
14
b
siCtl
siCtl L-NAME
siAdamts1
siAdamts1 L-NAME
AsAo
Maximal diameter (mm)
Days
****
ns
AbAo
su
c
Elastin breaks
L-NAME
siCtl
siAdamts1
d
Collagen content (%)
e
Mmp9
Mmp2
Enzymatic activity
f
Adamts1+/+
Adamts1+/+ L-NAME
Adamts1+/-
Adamts1+/- L-NAME
AsAo
AbAo
Maximal diameter (mm)
Days
g
Systolic BP (mmHg)
Adamts1
Control
L-NAME
h
Elastin breaks
i
Collagen content (%)

Figure 4

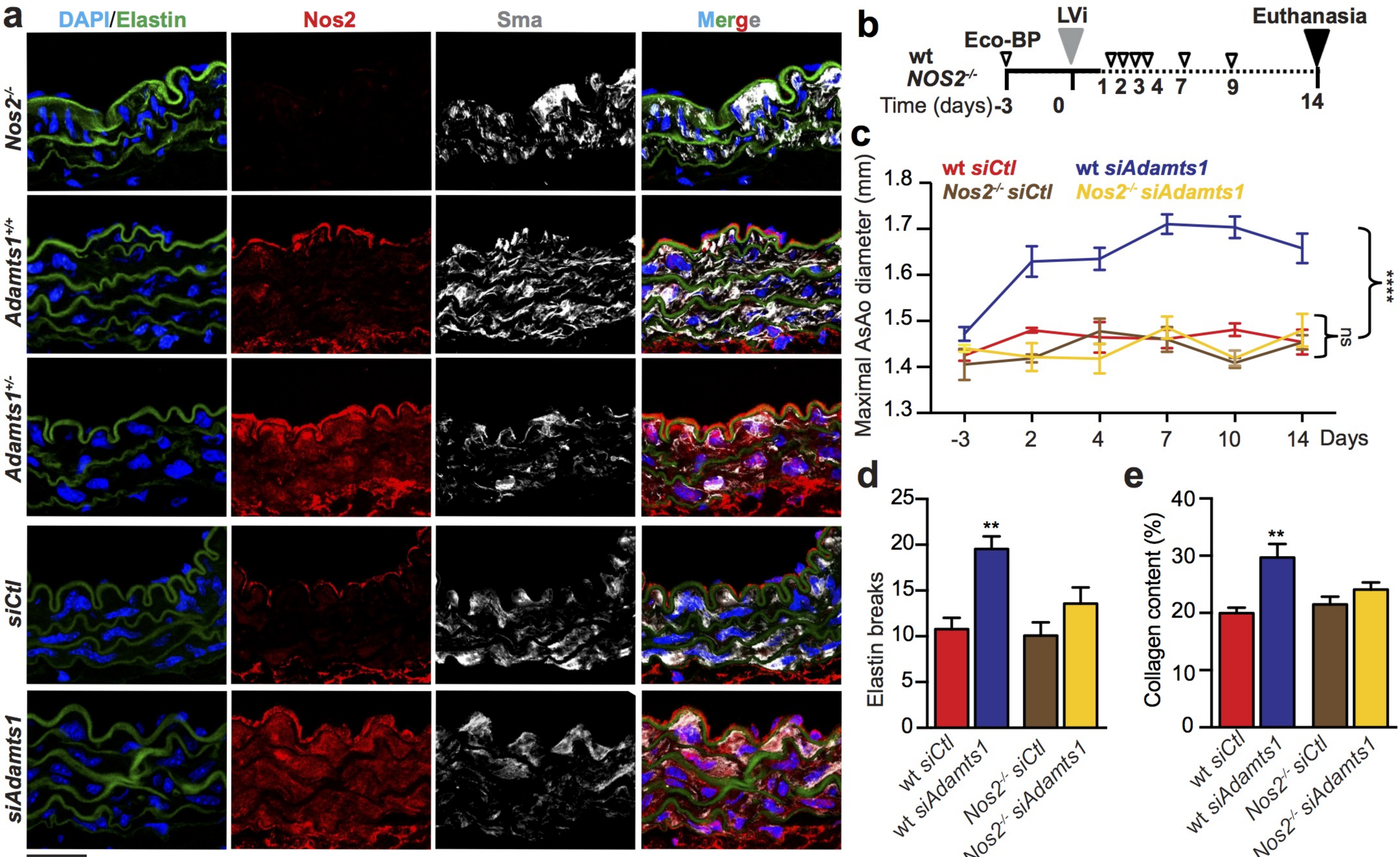
a
DAPI/Elastin
Nos2
Sma
Merge
Nos2-/-
Adamts1+/+
Adamts1+/-
siCtl
siAdamts1
b
wt
NOS2-/-
Eco-BP
LVi
Euthanasia
Time (days) -3 0 1 2 3 4 7 9 14
c
wt siCtl
wt siAdamts1
Nos2-/- siCtl
Nos2-/- siAdamts1
Maximal AsAo diameter (mm)
1.8
1.7
1.6
1.5
1.4
1.3
-3 2 4 7 10 14 Days
ns
****
d
Elastin breaks
25
20
15
10
5
0
**
wt siCtl
wt siAdamts1
Nos2-/- siCtl
Nos2-/- siAdamts1
e
Collagen content (%)
40
30
20
10
0
**
wt siCtl
wt siAdamts1
Nos2-/- siCtl
Nos2-/- siAdamts1
f
wt siCtl
wt siAdamts1
Nos2-/- siCtl
Nos2-/- siAdamts1
Systolic BP (mmHg)
130
120
110
100
90
80
-3 2 4 7 10 14 Days
ns
****
g
wt siCtl
wt siAdamts1
Nos2-/- siAdamts1
Adamts1+/+
Adamts1+/-
NO
h
siCtl
siAdamts1
p-Akt-S473
Akt
p-p65
p65
Gapdh
i
Adamts1+/+ vehicle
Adamts1+/+ AZD8055
Adamts1+/- Vehicle
Adamts1+/- AZD8055
Maximal aortic diameter (mm)
AsAo
AbAo
****
****
0 2 4 0 2 4 Days
j
Systolic BP (mmHg)
140
130
120
110
100
90
80
**
****
Adamts1 +/+ +/- +/+ +/-
Control
AZD8055
k
Nos2 mRNA levels
6
4
2
0
**
###
AZD8055 - + - +
Adamts1+/+
Adamts1+/-
l
Adamts1+/+
Adamts1+/-
NO
Vehicle
AZD8055

Figure 5

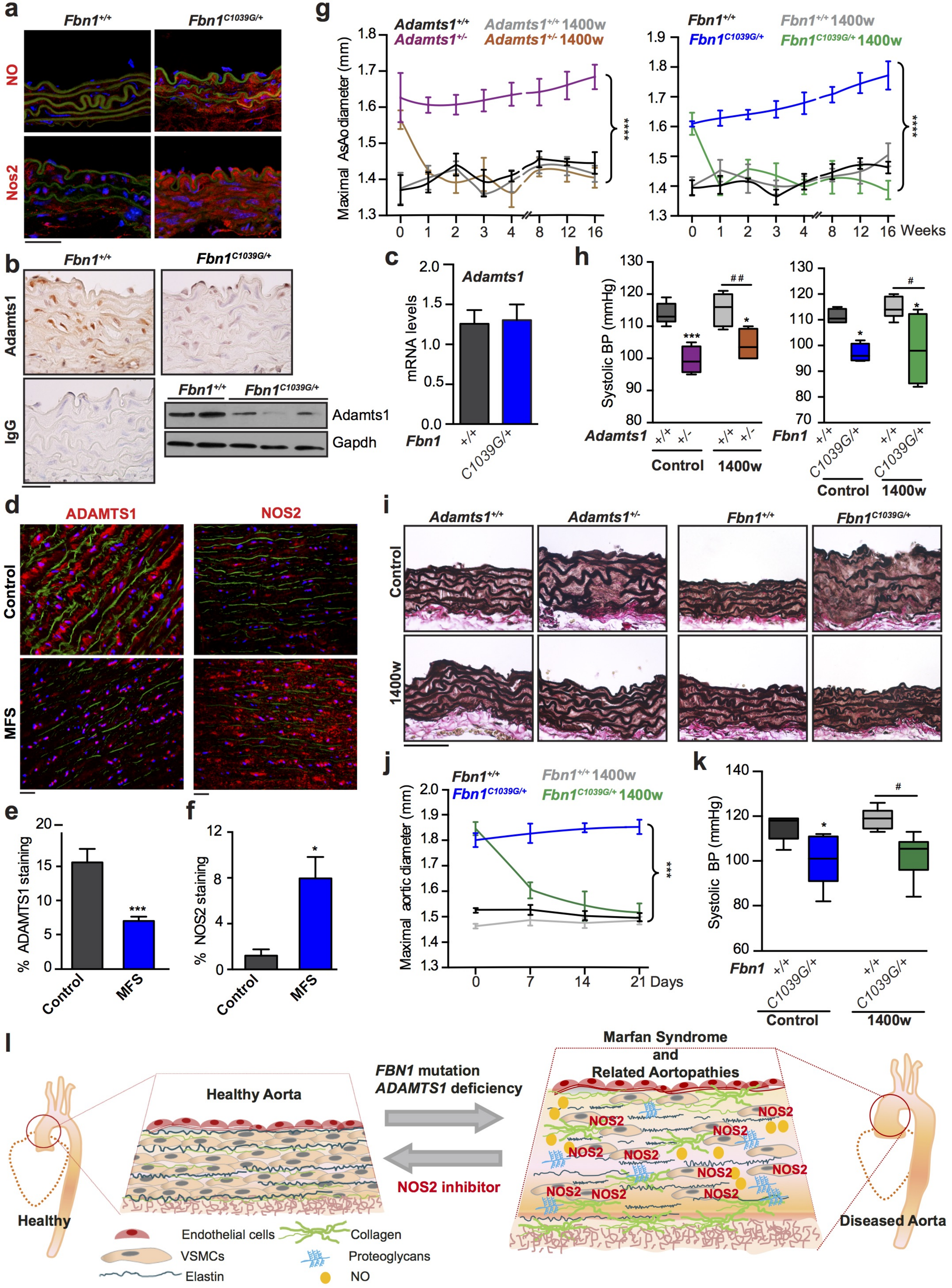
a
Fbn1+/+
Fbn1C1039G/+
NO
Nos2
b
Fbn1+/+
Fbn1C1039G/+
Adamts1
IgG
Fbn1+/+
Fbn1C1039G/+
Adamts1
Gapdh
c
Adamts1
mRNA levels
Fbn1
+/+
C1039G/+
g
Adamts1+/+
Adamts1+/-
Adamts1+/+ 1400w
Adamts1+/- 1400w
Maximal AsAo diameter (mm)
****
Fbn1+/+
Fbn1C1039G/+
Fbn1+/+ 1400w
Fbn1C1039G/+ 1400w
****
Weeks
h
Systolic BP (mmHg)
Adamts1
Control
1400w
Fbn1
Control
1400w
d
ADAMTS1
NOS2
Control
MFS
e
% ADAMTS1 staining
Control
MFS
f
% NOS2 staining
Control
MFS
i
Adamts1+/+
Adamts1+/-
Fbn1+/+
Fbn1C1039G/+
Control
1400w
j
Fbn1+/+
Fbn1C1039G/+
Fbn1+/+ 1400w
Fbn1C1039G/+ 1400w
Maximal aortic diameter (mm)
Days
k
Systolic BP (mmHg)
Fbn1
Control
1400w
l
Healthy
Healthy Aorta
FBN1 mutation
ADAMTS1 deficiency
NOS2 inhibitor
Marfan Syndrome
and
Related Aortopathies
Diseased Aorta
Endothelial cells
VSMCs
Elastin
Collagen
Proteoglycans
NO

Figure 6